AE-418
UDC 533.9.082.5:
546.291

AE-418

Measurements of the Spectral Light Emission from Decaying High Pressure Helium Plasmas.

J. Stevefelt and J. Johansson

AKTIEBOLAGET ATOMENERGI

STUDSVIK, NYKÖPING, SWEDEN 1971

MEASUREMENTS OF THE SPECTRAL LIGHT EMISSION FROM DECAYING HIGH PRESSURE HELIUM PLASMAS

J Stevefelt and J Johansson

ABSTRACT

The rate of electron density decay has been determined in a helium pulsed discharge plasma at pressures ranging from 100 to 600 Torr, primarily during the early afterglow where the electron density is from 10^{19} to $2 \cdot 10^{17}$ m^{-3}. Measurements of the electrical conductivity and the absolute intensity of the light emission were made. The effective recombination rate coefficient was found to increase faster than linearly with gas pressure. The total photon emission rate was significantly lower than the effective recombination rate. Below 400 Torr pressure the afterglow was dominated by He_2 bands, which were related to the recombination of He_2^+ and He_3^+ ions. At higher pressures the appearance of intense lines originating from the atomic n = 3 and 2^3P states is proposed to result from the He_4^+ recombination. Absorption measurements of the atomic metastable concentration gave evidence for recombination directly into the 2^3S state. The concentration of molecular metastables was surprisingly low. The light emission had a $T_e^{-\chi}$ dependence, with $0 < \chi < 0.35$ for the intense atomic lines and $0.78 < \chi < 1.10$ for the molecular bands.

Research supported by the Swedish Board for Technical Development

---

Printed and distributed in April, 1971

LIST OF CONTENTS

I. INTRODUCTION

In spite of the large number of experiments performed on the decay of helium afterglow plasmas, there are still important gaps in the understanding of all the underlying phenomena. Only at low gas pressures ($\lesssim$ 1 Torr), when the dominant ion is the atomic He^+, are the experimental results in reasonable agreement with the theory of collisional-radiative recombination[1]. When the gas pressure is higher, molecular helium ions are formed, and the recombination processes become more complex. It was recognized[2] that the spectral band emission, radiated by He_2 molecules in bound excited states, is caused by the collisional-radiative recombination of He_2^+ ions.

The recombination rate coefficient was found[3, 4] to have one component proportional to the gas density, in the pressure range 10 - 760 Torr, which was interpreted as a three-body recombination of He_2^+ stabilized by neutral helium atoms[5]. However, other studies[6] of a helium afterglow at the pressure 44.6 Torr have demonstrated serious unexplained deviations from the collisional-radiative model of three-body recombination. Recently it has been shown[7, 8] that the more complex ions He_3^+ and He_4^+ exist in high pressure helium plasmas at room temperature, and that these may give rise to the pressure-dependent component of the recombination rate coefficient.

The present experiment was initiated in order to extend the investigated pressure regime up to atmospheric pressure. In the studies to be reported here, the gas temperature was kept in the range between 300°K and 600°K. The main purpose of this paper is to present the results of light intensity and conductivity measurements made on pulsed afterglow plasmas in this regime, and to discuss some mechanisms which may be responsible for the observed phenomena.

II. EXPERIMENTAL EQUIPMENT AND TECHNIQUES

In principle the measurements are performed in the following manner. A high voltage (up to 2 kV) initiates a pulsed discharge between two electrodes in high-purity helium gas flowing through a discharge chamber. After a certain time (typical value 50 μsec) the discharge circuit is interrupted and the resultant afterglow studied by means of time-resolved spectroscopy and conductivity measurements. The discharge repetition rate is 50 or 100 sec^{-1}.

The block diagram of the experimental device is given in Figure 1.

Two different gas-handling systems and discharge chambers, which could be connected to a common electronic and diagnostic system, were used. In some of the experiments the plasma was generated between a stainless steel anode and a thermionically emitting tungsten cathode, mounted 23 mm apart, inside a stainless steel cross tube provided with two windows (quartz and sapphire) for optical measurements. In this case the helium gas was heated by the cathode to 500 - 600°K temperature, as measured with a thermocouple. The discharge chamber, together with its valves and connexions, was vacuumbaked at maximum 400°C, after which a pressure of 10^{-9} Torr or less could be attained. The helium gas was led into the discharge chamber through a heated quartz diffusion cell, and a continuous gas flow of about 4 atm. -litres per hour was maintained. The only impurity present in the afterglow emission spectrum was hydrogen, whose spectral line H_α was about 1 - 5% of the intensity of the helium line at 5876 Å.

In order to increase the helium flow rate and further suppress the outgassing of impurities, another system was developed. The cleanest gas was obtained with a purification system consisting of a calcium filter, a hopcalite furnace, and a cold trap at liquid nitrogen temperature. This purifier was connected to a discharge chamber made of glass, in which

a special type of cathode was used in order to create a plasma of larger diameter. The cathode consisted of an auxiliary pulsed glow discharge, struck between a straight tungsten wire and a surrounding tungsten helix of inner diameter 1.5 mm. The main discharge was drawn to a stainless steel anode, situated 20 mm from the "plasma cathode", and had an effective diameter of about 4 - 5 mm, which made possible spatially resolved measurements of the light emission. In this arrangement the gas heating was negligible, and the gas temperature was close to 300°K. The gas purity was considerably improved relative to the first system, especially at higher pressures.

After cessation of the active discharge, small subsidiary current pulses could be passed between the anode and the cathode for two purposes: to determine the plasma conductivity and to elevate the electron temperature selectively. The magnitude of the current was determined by measuring the voltage drop over a known series resistance, while the electric field was measured between two floating probes inserted into the plasma column, 6.6 mm apart. In order to obtain the local current density and conductivity, a relation between the plasma light emission and its electron density was assumed to exist. The slit of a grating spectrometer was focussed onto the plasma column and could be traversed across the column to obtain the light intensity as a function of transverse position. These data were then inverted to radial intensity, and the emission in the helium line at 5876 Å was assumed to be proportional to the square of electron density. This assumption is only approximately correct, as will be shown later.

The spectrometer (Czerny - Turner 1 m) was provided with a photomultiplier, and single photoelectrons were counted on a scaler. This counting system was turned on at a preset delay time after each discharge, and stayed open during a preset gate time. In this manner time sampled

light detection was achieved. By using a tungsten ribbon filament lamp as a standard, the spectrometer-photomultiplier combination was calibrated for absolute intensity measurements of the plasma afterglow emission in the spectrum range between 2500 and 11000 Å.

Irradiating the plasma with intense light from a pulsed Philips helium lamp, the absorption of light by helium atoms in the metastable state 2^3S could be measured. The magnitude of the light absorption will become a function of the line shapes of both the impinging and the absorbed radiation, as well as the density of absorbing atoms at different positions along the light path. The spatial distribution of metastables was determined from measurements of the absorption at different transverse positions in a manner similar to that used for the emission measurements.

III. MEASUREMENTS AND RESULTS

A. Conductivity measurements

Over the complete pressure interval investigated in this study (100 - 600 Torr), the measured transverse profiles of the light emission appear to be independent of the delay time, during the first 60 μsec of the afterglow where accurate spatially resolved measurements could be made. Hence the geometrical form factor, used to evaluate the local conductivity on the center line of the plasma column from the measured over-all conductance, is assumed to be constant in time. This form factor has here the dimension of an effective cross section of the plasma column, and may be experimentally determined only within a factor of two. This sets a lower limit of error for this method of measuring the electron density. Its general reliability was tested at a pressure of 10 Torr, where the population densities of highly excited levels (n = 10 - 15) of the helium atom could be simultaneously measured[9] and found to be

in Saha equilibrium with the free electrons at the electron temperature, thus providing an independent determination of the electron density.

The obtained values of the conductivity lie in the range between 15 and 0.0001 mhos/m. The conductivity resulting from the interaction of electrons with other charged particles is, according to Spitzer's expression[10], equal to about 30 mhos/m at an electron temperature $T_e = 300^oK$ and with a value of the Coulomb logarithm $\ln\Lambda \approx 3$. Electron-ion collisions would then be of importance for the plasma conductivity only during the very early afterglow, and were neglected in the following since the electron temperature is not accurately known (if T_e is elevated, the electron-ion conductivity becomes larger proportional to $T_e^{3/2}$, and its relative contribution to the total conductivity consequently smaller).

By using a constant cross section $Q = 5.3 \cdot 10^{-20}$ m^2 for momentum transfer in collisions between electrons and helium gas atoms, we obtain the following expression for the electrical conductivity of the plasma:

$$\sigma = 7.26 \cdot 10^7 \frac{N_e}{N_a T_e^{1/2}} \text{ mhos/m} \qquad (1)$$

where N_e and N_a are the densities of free electrons and gas atoms, respectively. This expression is used to calculate the electron density N_e from the experimentally determined conductivity σ, assuming T_e is governed mainly by the applied electric field (equation (7) below).

A typical experimental result is illustrated in Figure 2 for 388 Torr gas pressure and a gas temperature near 300^oK. The bars indicated on the plots represent the estimated error of the measurement, where systematic errors in the geometrical form factor for later times than 60 μsec have not been taken into account. From the electron densities, evaluated at different delay times, an effective recombination rate coefficient

could be determined according to the differential equation

$$\frac{dN_e}{dt} = - \alpha_{eff} N_e^2 \qquad (2)$$

with the solution (α_{eff} being independent of time t):

$$N_e^{-1} = \alpha_{eff} t + N_{eo}^{-1} \qquad (3)$$

In Figure 3 we have plotted N_e^{-1} versus time for five different gas pressures, and the slopes of these plots would then represent the values of α_{eff}. Even if the found values vary with time in the afterglow, it is seen that the effective recombination rate increases significantly with gas pressure. After a transition time of varying length in the very early afterglow, there exists a time interval where α_{eff} is almost constant. At delay times later than 50 μsec, α_{eff} again increases with time; this may occur rather suddenly as illustrated in Figure 4 for 388 Torr gas pressure, or sometimes more gradually.

From the linear parts of the N_e^{-1} plots, before 50 μsec delay time, the effective recombination rate coefficients obtained at different gas pressures are shown in Figure 5. Previously published results[3, 4, 6] are also shown for comparison. It appears that the monotonic increase of the effective recombination coefficient with pressure occurs even faster than linearly at pressures greater than about 100 Torr. The possible reason for these observed phenomena will be discussed in section IV A.

B. Absolute intensity measurements of atomic light

It is a very well known fact that helium afterglow spectra at high pressures are dominated by intense He_2 bands. However, even in the pressure range studied here, there still exist spectral lines emanating

from radiative transitions between excited states of the helium atom. At lower pressures the source of this line radiation has been convincingly shown by several experiments to be the collisional-radiative recombination of atomic He^+ ions, with a significant amount of light being emitted also in transitions from highly excited atomic energy levels. The same relative distribution over excited levels with principal quantum numbers $n \geq 4$ appears to be approximately valid also at pressures above 100 Torr, although the absolute intensities are weaker so that radiative transitions from states higher than 10^3D cannot be observed with our equipment.

All transitions from atomic excited states with principal quantum number $n = 3$ become more intense relative to the lines from higher levels, as compared with an afterglow spectrum at low pressure. The effect is most pronounced for the line $3^3D - 2^3P$ at 5876 Å, and increases with increasing pressure, as illustrated in Table 1 for the spectral series $n^3D - 2^3P$. All atomic lines were found to decay similarly, so that their relative intensities remain essentially unchanged at different times in the afterglow.

Also the intensity of the infrared line $2^3P - 2^3S$ at 10 830 Å increases relative to the lines emitted from the quantum levels $n \geq 4$ when the pressure is elevated, which could be expected since this transition constitutes a subsequent cascading of the lines $3^3S - 2^3P$ and $3^3D - 2^3P$. However, the important observation is made that the number of radiative transitions, per cubic meter and second, departing from the state 2^3P, is about a factor 2.5 larger than the number of radiative transitions arriving at this level, at all pressures above 100 Torr. For comparison measurements at 6 Torr pressure resulted in a corresponding value for this ratio equal to 1.25 - the deviation from unity is here within the limits of error for the absolute intensity calibration of the spectrometer recording system.

The rate of photon emission in the 5876 Å line constitutes about 50% of the total atomic photon emission rate in the visible wavelength range, and at all pressures above 100 Torr it could be related to the electron density through the approximation

$$I_{5876} = A\, N_e^{\,b} \qquad (4)$$

where A and b are functions of pressure only. This is illustrated in Figure 6, where the logarithm of I_{5876} plotted versus the logarithm of N_e gives straight lines. The slope b of these lines is between 1.4 and 2.2, and for a constant electron density the intensities of the atomic helium lines increases rapidly with the gas pressure up to a maximum at about 460 Torr, and then decreases with further elevation of pressure.

C. Absolute intensity measurements of molecular light

The absolute intensities of the molecular He_2 bands were determined by slowly scanning the spectrometer with resolution of the order 1 Å over the band. In this manner the light distribution over the different rotational lines was obtained on a pen recorder, and at the same time the total band intensity was obtained by integrating the number of photon counts on a scaler. The rotational distribution was found to correspond to a temperature $T_{rot} \simeq 800^{\circ}K$ at all gas pressures, and the intensity sum of all individual rotational lines of the $3p^3\Pi_g - 2s^3\Sigma_u^+$ band was a factor 17.0 times larger than the Q(7) component at 4653 Å, as obtained from the pen record. The integrated number of photon counts over the wavelength interval 4625 - 4750 Å resulted in a band intensity that was 23.3 times larger than the Q(7) intensity (after subtraction of the atomic line at 4713 Å, but including also the weak (1,1)-transition).

The decays of four molecular bands ($3p^3\Pi_g - 2s^3\Sigma_u^+$, $4p^3\Pi_g - 2s^3\Sigma_u^+$, $3d^3\Sigma_u^+$, $^3\Pi_u$, $^3\Delta_u - 2p^3\Pi_g$, and $4d^3\Sigma_u^+$, $^3\Pi_u$, $^3\Delta_u - 2p^3\Pi_g$) could be followed out to 50 μsec in the afterglow, and were found to be nearly alike. The relative intensities of the different bands were found to be similar to those of the corresponding transitions in the atomic helium spectrum at low pressures, and the intensity of the $3p^3\Pi_g - 2s^3\Sigma_u^+$ band constituted 9.5% of the sum of eleven molecular band intensities, measured in the early afterglow. This summed intensity was estimated to constitute 88% of the total He_2 band radiation in the visible wavelength range, and hence this total molecular photon emission rate I_{mol} is a factor 280 times larger than the rate of photon emission in the Q(7) line at 4653 Å. Care was taken to determine this factor accurately, and it can be noted that our value is about 6.2 times smaller than the value found by Kerr et al.[11] for the Q(5) line at $T_{rot} = 515^oK$.

The molecular He_2 bands decay at a slower rate than the atomic lines do. Their intensities may be related to the electron density through an expression of the same form as equation (4), which is demonstrated in Figure 7 for the rotational line Q(7) of the 4650 Å band. Here the slower decay rate of the molecular bands shows up in a smaller value for the exponent b, being between 0.7 and 1.0. Like the atomic lines, the He_2 bands also become more intense with increasing pressure up to a maximum around 400 - 450 Torr, after which their intensities diminish. The pressure variations are smaller, though, than for the atomic lines, and in particular the intensity rise is much larger for the lines, when the gas pressure is increased from 200 to 400 Torr, so that there occurs a very evident shift towards a spectrum dominated by atomic helium lines in the early afterglow at pressures above 400 Torr. In Figure 8 the relationship between atomic and molecular light emission is shown: its exponential

character is a direct consequence of the fact that both kinds of emission obey the equation (4).

If the light emission were proportional to the recombination rate,

$$I = K \alpha N_e^{\,2} \tag{5}$$

where the time dependence of N_e is given by equation (3), then the time variation of the light emission could be expressed as

$$I^{-1/2} = \frac{\alpha_{eff}}{(K\alpha)^{1/2}} t + \frac{1}{(K\alpha)^{1/2} N_{eo}} \tag{6}$$

Despite that the molecular bands do not obey the equation (5), their time dependence is very well described by analytical expressions of the form given in equation (6), as illustrated in Figure 9. The contradiction between the equations (6) and (4) with $b \neq 2$ will be further discussed in section IV C.

The slope of the straight lines in Figure 9 increases with gas pressure, reflecting a faster decay rate of the molecular bands at higher pressures. In Figure 10 the pressure variation of the time derivative of $I_{4653}^{-1/2}$ ($Q(7)$ line of the 4650 Å band) is shown graphically. Also shown in this Figure is the result reported by Collins[6] for a helium afterglow at 44.6 Torr pressure, where the dotted bar indicates variation with electron density. The solid bars, attached to the results from this study, represent estimated errors only. The similarity between this Figure and Figure 5 for α_{eff} is obvious, and will be discussed further in section IV C.

D. Absorption Measurements

The measured absorption of light at 3889 Å ($2^3S - 3^3P$ transition of the helium atom), traversing the plasma column along a diameter,

amounts to between 3 and 25% during the first 50 μsec of the afterglow. The corresponding absorption at 10 830 Å ($2^3S - 2^3P$ transition) is between 25 and 80%.

The absorption at 3889 Å wavelength was used to evaluate the number density of atoms in the metastable state 2^3S, and the result is shown in Figure 11 for different gas pressures and times in the afterglow. The metastable density appears to decay almost exponentially with the same characteristic time 23.5 μsec at all pressures, and the relative densities at the three pressures 200, 388, and 578 Torr are approximately in the ratio 6:13:4, respectively.

For light of the wavelength 4653 Å, corresponding to the Q(7) line of the $2s^3\Sigma_u^+ - 3p^3\Pi_g$ band, the absorption of the plasma in the transverse direction was smaller than 1%, and could not be detected with our equipment. This implies that the number density of He_2 molecules in the metastable state $2s^3\Sigma_u^+$ must be smaller than 10^{18} m^{-3} at all gas pressures and times in the afterglow.

E. Influence of elevated electron temperature

When a small electric dc field E is applied to a plasma, having such a degree of ionization that the electronic energy distribution will be nearly Maxwellian but Coulomb collisions can be neglected, the electron temperature is governed by an energy balance between the Joule heat and elastic losses in electron-atom collisions. Using again an energy-independent cross section $Q = 5.3 \cdot 10^{-20}$ m^2 for the electron-atom momentum transfer in helium, the ratio $\theta = T_e/T_a$ between the electron and gas temperatures will be given by the expression

$$\theta(\theta - 1) = 0.31 \left(\frac{E}{p}\right)^2 \qquad (7)$$

where p is the (real) gas pressure in Torr, and E is expressed in volts/meter. The recombination energy, imparted to the electrons in the afterglow, has been neglected in the energy balance equation (7).

The method of selective heating of the free electrons has been employed by several experimenters to study the electron temperature dependence of recombination processes. The collisional-radiative recombination is characterized by a strong dependence, theoretically like $T_e^{-4.5}$, on electron temperature, so that a moderate ratio of electric field to pressure (E/p) will cause an effective diminution of the recombination rate in helium at low pressures. This is the well-known phenomenon of "afterglow quenching".

The influence of an electron temperature elevation, induced by short current pulses of different amplitudes, on the light emission in some spectral lines and one He_2 band in the afterglow, at a (reduced) gas pressure p_o = 88 Torr, is shown graphically in Figure 12. The heating pulse is applied between 5 and 25 μsec after the end of the active discharge, and the photomultiplier gate is opened during a part of the pulse, or between 10 and 20 μsec after the discharge cessation. Only the impurity hydrogen H_β line at 4861 Å is strongly quenched by the heating pulse, while the helium molecular band at 4650 Å diminishes with increasing electron temperature like $T_e^{-1.10}$. The helium atomic line at 5876 Å is rather weakly quenched, approximately like $T_e^{-0.35}$, and starts increasing in intensity at about $T_e = 6000^oK$, probably due to the onset of excitation processes. The infrared helium line at 10 830 Å, finally, is not quenched at all, but increases monotonically with electron temperature. For small electric fields the obtained results deviate from the straight lines, drawn in the figure, which may be due to the omission of the heating by recombination processes in equation (7).

At a higher gas pressure of 380 Torr, the diminution of the 4650 Å band intensity with rising electron temperature is still somewhat slower, like $T_e^{-0.78}$, while the 5876 Å line remains essentially unaffected up to $T_e = 6000^oK$, where it starts increasing.

The results of time-resolved intensity measurements of the two atomic helium lines at 5876 Å and 10 830 Å, and the molecular He_2 band at 4650 Å, are illustrated in Figure 13, a - c. These measurements were made at a gas pressure $p_o = 165$ Torr and a gas temperature 510^oK. A 10 μsec duration electron heating pulse was applied, which would elevate the electron temperature to 2300^oK. Its influence on the light emission is shown, and for comparison also the decay curves when no pulse is applied. The 5876 Å line exhibits a very small change during the pulse, but its intensity rises by a factor 1.8 when the heating pulse is interrupted. The infrared 10 830 Å line increases immediately in intensity when the electron heating pulse begins, and then decays back to its nominal value. After pulse cessation a slight intensity rise occurs. Finally, the 4650 Å band becomes quenched by the pulse to about 40% of its normal value, and after the pulse the band intensity rises to about twice its normal value.

IV. DISCUSSION AND CONCLUSIONS

A. Electron density decay

We shall start the discussion of the experimental results with an order-of-magnitude estimate of the ambipolar diffusion rate. From the measured transverse light emission profiles we derive a radial electron density profile, which is similar to a first-order diffusion profile with a characteristic diffusion length Λ typically about 0.2 cm. If we assume a value $D_a p_o = 700$ cm^2 · Torr/sec, where D_a is the ambipolar diffusion

coefficient, we obtain at the gas pressure p_o = 100 Torr a characteristic ambipolar diffusion loss frequency $\nu_d = D_a/\Lambda^2$ = 175 sec^{-1}. It is immediately seen that this value is much smaller than the effective loss frequency for the electrons, which is of the order 10^4 sec^{-1} or more.

A recombination controlled afterglow with an initial radial diffusion profile gradually develops into a recombination profile with time, that is into a homogeneous plasma. The effective diameter of the plasma column then increases with time, as a consequence of the recombination law, equation (2). The observed time independence of the radial electron density profile, though, implies a rate equation of the form

$$\frac{dN_e}{dt} = - \nu_e N_e \qquad (8)$$

where ν_e is a constant. This equation is identical with the equation (2) if

$$\alpha_{eff} = \frac{\nu_e}{N_e} \qquad (9)$$

Such a dependence of the effective recombination rate coefficient α_{eff} on electron density N_e might in fact result from an electron temperature elevation for higher densities N_e, so that the electron temperature is higher on the center line of the plasma column than it is at some distance out. However, equation (9) is contradictory to the observed time independence of α_{eff} during part of the early afterglow, as presented in Figure 3.

The time history of the inverse electron density N_e^{-1}, displayed in Figure 3 for different pressures, may be divided into three characteristic parts. The first part is characterized by a small (but gradually increasing) recombination rate coefficient, which may be due to the

electron temperature elevation mentioned above, or to ionizing metastable-metastable collisions, or to both these together since the paired metastable collisions produce energetic electrons (processes (13) and (14) below).

During the second part of the afterglow the effective recombination rate coefficient α_{eff} is constant, and its value is a monotonically increasing function of gas pressure, as shown in Figure 5. Our results from this part of the afterglow fit quite well previously reported values[3, 4, 6] and further, the linear dependence of α_{eff} on pressure for not too high degrees of ionization in the pressure range 10 - 100 Torr seems to develop into a more quadratic dependence at higher gas pressures. Such a deviation from the linear pressure dependence has recently been predicted[7] for high-pressure helium plasmas, due to the recombination of electrons with the He_4^+ ion.

The last part of the afterglow starts at delay times around 40 - 50 μsec. The graph of N_e^{-1} versus time, as measured at the gas pressure 388 Torr and illustrated in Figure 4, shows a sudden change for the value of α_{eff} from $5.5 \cdot 10^{-14}$ m^3/sec at earlier delay times to $(1.0 \pm 0.1) \cdot 10^{-12}$ m^3/sec at delay times later than 50 μsec. We propose that this is due to a change in the relative concentrations of different kinds of ions, but the reasons for this change are presently unknown. One hypothesis is that this last part of the afterglow is dominated by the electron-ion recombination of the ion He_4^+.

From the data presented by Gusinow et al.[7] we take the following values for the equilibrium constants between the relative concentrations of the three molecular helium ions He_2^+, He_3^+, and He_4^+ at 300°K gas temperature:

$$\frac{[He_2^+]^*[He]^*}{[He_3^+]^*} = 6 \cdot 10^{26}\ m^{-3} \qquad (10)$$

$$\frac{[He_3^+]^*[He]^*}{[He_4^+]^*} = 1 \cdot 10^{24}\ m^{-3} \qquad (11)$$

where the brackets indicate densities and the asterisks indicate equilibrium conditions. By means of these relations the relative ion concentrations can be calculated for different gas pressures, and the result is illustrated in Figure 14. It is seen that the relative concentration of the He_3^+ ion increases with pressure to a maximum value of 2% at 760 Torr pressure. At the same pressure the relative amount of He_4^+ has increased to the same value as He_2^+, or 49% of each. At still higher pressures the relative concentration $[He_4^+]$ tends to unity, while $[He_2^+]$ and $[He_3^+]$ decrease to zero. It may be noted from equation (11) that already for pressures $p_o > 31$ Torr, $[He_4^+]$ becomes larger than $[He_3^+]$ under equilibrium conditions.

B. Light emission. Atomic spectrum

Next we shall proceed by considering the light emission from the recombining high-pressure helium plasmas. It will be shown that this gives additional evidence that the minority ions He_3^+ and He_4^+ play an active role in such afterglows.

Since the atomic helium energy level 10^3D lies at least 2 eV above the ground state of all the molecular helium ions, the observed existence of excited atoms in this level probably results from the recombination of atomic He^+ ions. These ions are at higher pressures known to convert rapidly into molecular He_2^+ ions via the three-body process

$$He^+ + 2\ He \rightarrow He_2^+ + He \qquad (12)$$

which is the reason for the predominance of intense He_2 bands in helium afterglows at pressures above 10 Torr, presumably originating in part from the recombination of He_2^+ ions. The reaction rate coefficient for the process (12) can be expressed as βp_o^2, and reported values for β lie in the range from[12] 78 $Torr^{-2}sec^{-1}$ to[13] 109 $Torr^{-2}sec^{-1}$. These values lead to a characteristic conversion time of 0.3 μsec at a gas pressure p_o = = 200 Torr, which is at least a factor 20 faster than the observed decay time for the atomic line radiation. The discrepancy might imply that the reported values for β are too large, but we are more inclined to assume that there exists a source of atomic ions in the afterglow, due to mutual collisions between metastable atoms and molecules[14, 15]:

$$2\ He\ (2^3S) \rightarrow He^+ + He + e \qquad (13)$$

$$2\ He_2\ (2^3\Sigma_u^+) \rightarrow He^+ + 3\ He + e \qquad (14)$$

The reaction rate coefficients for these two processes have been found[15] to be about equal ($\simeq 1.8 \cdot 10^{-15}$ m^3/sec), and since the concentration of molecular metastables in the present experiment is at least one order of magnitude smaller than the concentration of atomic metastables, the process (14) could be neglected in this context.

The population density of the excited energy level 10^3D is of the order 10^{13} m^{-3} (summed over the 15 degenerate sublevels) in the early afterglow, where the electron density is about 10^{19} m^{-3}. No certain conclusion about the concentration $[He^+]$ of atomic ions can be drawn from this, though, since no equilibrium between this excited level and the free states could be proved to exist.

Two different mechanisms might be responsible for the observed increase in population density of the atomic n = 3 states and the 2^3P state relative to the other states, as the gas pressure is risen. These are:

a. excitation from the metastable atomic state 2^3S by collisions with hot electrons produced in metastable-metastable collisions, or
b. dissociative recombination of a molecular helium ion, where the fragments after the recombination could be helium atoms in the ground state and in excited n = 2 or n = 3 states.

Since the concentration of atomic metastables does not rise with pressure, the mechanism a. must imply that instead the rate coefficient for metastable-metastable collisions increases with pressure. This could be the case if the reaction proceeds according to

$$2\ He\ (2^3S) + He\ (1^1S) \rightarrow He_2^+ + He + e \qquad (15)$$

as was demonstrated[16] for a helium afterglow at liquid nitrogen temperature. The rate of production of hot electrons, having a mean energy of about 10 eV, might be assumed to be of the same order of magnitude as the effective recombination rate, or about $10^{25}\ m^{-3}sec^{-1}$ in the very early afterglow, if the reaction rate coefficient for the (hypothetical) process (15) is taken as large as $5 \cdot 10^{-39}\ m^6/sec$. A thermalization time for the electrons can be calculated from the expression given by Spitzer[10] to be about $2 \cdot 10^{-10}$ sec, and since the electron-atom collision frequency is about equal to $5 \cdot 10^{11}\ sec^{-1}$, each produced hot electron will collide with an order of 100 gas atoms during its thermalization time, but only a fraction $1:10^6$ of these atoms will be in the excited state 2^3S. Hence, the maximum rate of excitation from this state would be of the order

10^{21} $m^{-3}sec^{-1}$, which is still two orders of magnitude smaller than the rate of photon emission in the radiative transitions from the n = 3 and the 2^3P states during the very early afterglow (this means the first 10 μsec after discharge cessation).

Thus there remains the mechanism b. and the excess number of excited helium atoms in the lower quantum states should be the result of a dissociative recombination process. The cross section for dissociative recombination of the He_2^+ ion is now generally accepted to be negligible, but as no bound states of the neutral He_3 and He_4 molecules have been proved to exist, dissociative recombination seems to be the only possible break-up mechanism for the He_3^+ and He_4^+ ions.

C. Light emission. "Total" light

It is interesting to compare the total rate of photon emission with the effective recombination rate. In a pure collisional-radiative model one and only one photon is emitted per recombination event. This condition is established because radiative de-excitation dominates largely over collisional de-excitation for the lower excited levels of the neutral atom or molecule. Recycling via the process (13) or (14) could result in more than one emitted photon per recombination.

For the calculation of the total atomic light I_{at} we add the number of radiative atomic transitions in the visible wavelength range, but replace the sum of the two spectral series $n^3S - 2^3P$ and $n^3D - 2^3P$ with the number of transitions in the line $2^3P - 2^3S$ at 10 830 Å. The total molecular light I_{mol} is taken to be a factor 280 times the emission in the Q(7) component of the 4650 Å band. These evaluations are made for a typical electron density chosen as $N_e = 10^{18}$ m^{-3}. The effective recombination rates are taken from the slopes of the curves in Figure 3, and the results for different gas pressures are compiled in the Table 2. It is con-

cluded that the emission rate of atomic light I_{at} rises from less than 1 % at 200 Torr pressure to about 14% of the effective recombination rate $\alpha_{eff} N_e^2$ at 464 Torr pressure. Further pressure elevation to 578 Torr results in a weaker atomic light emission, or about 2% of $\alpha_{eff} N_e^2$. The emission rate of molecular light I_{mol} is found to be about 17% of the effective recombination rate in the pressure range 200 - 388 Torr (from the data published by Collins[6] for a 44.6 Torr afterglow we have derived a value of 20% for this ratio). For higher gas pressures the ratio of I_{mol} to $\alpha_{eff} N_e^2$ diminishes to a value of 1.8% at 578 Torr. A maximum of 0.3 emitted light photons (atomic and molecular) per recombination event is obtained at around 388 Torr pressure, but the majority of the recombinations are non-radiative, probably dissociative with metastable atoms and/or molecules as fragments. However, it may be noted that if we were to use the factor given by Kerr et al.[11] (which we do not find reasonable) instead of the factor 280 for calculating I_{mol} from the measured I_{4653}, we should get the ratio of I_{mol} to $\alpha_{eff} N_e^2$ nearly unity for gas pressures up to 388 Torr.

It would seem that the simultaneous validity of equation (3) for N_e and the equations (4) with $b \neq 2$ and (6) for I_{mol} is inconsistent. However, the relation (4) is only approximate, as it is derived from a doubly logarithmic plot. If the values of the slopes in Figure 9 are identified as $\alpha_{eff}/(K\alpha)^{1/2}$ according to equation (6), α_{eff} is taken from Figure 5, and K is put equal to 1/280, values are obtained for the "recombination coefficient" α which are smaller than α_{eff} in about the same ratios as were obtained for I_{mol} to $\alpha_{eff} N_e^2$. The ratio α/α_{eff} is given in the last column of the Table 2. Clearly, this ratio is constant as long as α_{eff} does not vary with time in the afterglow (and presupposing that the slope of $I_{mol}^{-1/2}$ versus time does not vary). On the other hand, the ratio of

I_{mol} to $\alpha_{eff} N_e^2$ varies in time like N_e^{b-2}, when α_{eff} is constant, so that the agreement between the two ratios is only approximate, and perhaps accidental.

It is concluded that the helium molecular band radiation seems not to be simply related to the electronic recombination of the He_2^+ ion. Gerardo and Gusinow[8] obtained a spectrum dominated by intense He_2 bands from an afterglow at 80°K and pressures up to 30 Torr, where the dominant ion was found to be He_3^+ by mass spectrometry. At delay times later than a few hundred microseconds in the afterglow they report all atomic radiation from principal quantum levels greater than n = 4 to be essentially absent. On the basis of the increased intensity in the radiative transitions from the n = 3 and 2^3P states relative to the other transitions, found in this study as the gas pressure is elevated, together with the predicted increase in the relative He_4^+ ion concentration (Figure 14), we propose that this line emission is due to the dissociative recombination of the He_4^+ ion. At the highest pressure 578 Torr, though, all light emission, both atomic and molecular, becomes weaker, a phenomenon which is presently not understood.

D. Metastables

A rate equation for the concentration M_1 of atomic metastables can be written, taking into account all known creation and destruction processes:

$$\frac{dM_1}{dt} = f_1 \alpha N_e^2 - \beta M_1 N_e - 2\gamma M_1^2 - \delta N_a^2 M_1 \qquad (16)$$

The coefficient f_1 is the fraction of recombining ions which terminate as atomic metastables, the term $\beta M_1 N_e$ represents electronic de-excitation,

$$He(2^3S) + e \rightarrow He(1^1S) + e + 19.8\ eV \qquad (17)$$

with a reaction rate coefficient[17] β of the order 10^{-15} m^3/sec, $2\gamma M_1^2$ is the rate of destruction via the process (13) with[15] $\gamma = 1.8 \cdot 10^{-15}$ m^3/sec, and the last term represents three-body conversion into molecular metastables[18]

$$He(2^3S) + 2\ He(1^1S) \rightarrow He_2(2^3\Sigma_u^+) + He(1^1S) \qquad (18)$$

with $\delta = 2.5 \cdot 10^{-46}$ m^6/sec.

If the creation term $f_1 \alpha N_e^2$ is put equal to the atomic light emission I_{at}, as defined above, then this term becomes negligible in comparison with the destruction terms. The decay curve for M_1 at 200 Torr gas pressure seems to represent approximately the destruction due to the processes in the rate equation (16) with no source term. At the two higher pressures, though, this destruction should proceed faster due to the three-body conversion, and a source term of the order $f_1 \alpha N_e^2 = 10^{23}\ m^{-3} sec^{-1}$ at 25 μsec delay time has to be added in order to account for the slow decay rate at 578 Torr pressure. This is of the same order of magnitude as $\alpha_{eff} N_e^2$, and implies a non-radiative recombination process terminating directly in the atomic metastable state.

From our data we find that a reduction of the effective recombination rate coefficient α_{eff} due to metastable-metastable collisions might occur only at the pressure 388 Torr, where the ratio M_1/N_e is large.

A rate equation could also be written for the concentration M_2 of molecular metastables:

$$\frac{dM_2}{dt} = f_2 \alpha N_e^2 - \beta M_2 N_e - 2\gamma M_2^2 + \delta N_a^2 M_1 \qquad (19)$$

The values of the rate coefficients β and γ are here similar to those for

the atomic metastables[15]. If the production rate $f_2 \alpha N_e^2$ is put equal to the total molecular radiation I_{mol}, this term will again be negligible as compared with the source from three-body conversion. Assuming $dM_2/dt \simeq 0$ leads to $M_2 \simeq 10^{19}$ m^{-3} in the early afterglow at the gas pressure 388 Torr, which is more than one order of magnitude larger than what could be observed. The reasons for this discrepancy are not clear.

E. Electron temperature dependence

The observed electron temperature dependence of the 4650 Å band intensity, illustrated in Figure 12, is in rather good agreement with the reported[8] electron temperature dependence $T_e^{-\chi}$, $0.98 < \chi < 1.60$, of the recombination coefficient for the He_3^+ ion. The small difference between our obtained values for χ at the two gas pressures 88 and 380 Torr may be due to a component of molecular band radiation originating from He_2^+ recombination at the lower pressure, having a larger electron temperature dependence χ.

Similarly, the weak quenching of the atomic 5876 Å line at 88 Torr gas pressure may belong to the component originating from the recombination of atomic He^+ ions, while the line emission originating from He_4^+ recombination has almost no electron temperature dependence.

The rate coefficient for electronic excitation of the level 2^3P from the metastable level 2^3S is, as calculated with the Gryzinski[19] formula, equal to $7.8 \cdot 10^{-19}$ m^3/sec for $T_e = 0.1$ eV, and equal to $6.8 \cdot 10^{-15}$ m^3/sec for $T_e = 0.3$ eV. Hence, even a slight electron temperature elevation will result in excitation of the 2^3P level in the early afterglow, where $N_e \simeq M_1 \simeq 10^{19}$ m^{-3}, and give rise to the observed intensity increase in the 10 830 Å line. The reason for the intensity decay during the heating pulse is somewhat obscure, but may be some kind of normal

recombination quenching.

V. SUMMARY

Afterglow plasmas produced by a pulsed discharge in helium at pressures 100 - 600 Torr were found to decay according to a rather complex scheme involving recombination between electrons and several kinds of helium ions. The effective recombination rate coefficient during the first 50 μsec of the afterglow, where the electron density is in the range $2 \cdot 10^{17} < N_e < 10^{19}$ m^{-3}, was found to increase with gas pressure faster than linearly. For delay times later than 50 μsec the effective recombination rate coefficient increased also with time in the afterglow.

Spectral line emission from excited helium atoms up to principal quantum level n = 10 was observed, and ascribed to the collisional-radiative recombination of atomic helium ions, produced in metastable-metastable collisions. The lines originating from atomic n = 3 levels, as well as the 10 830 Å line from the 2^3P level, were all anomalously intense as compared with a low pressure afterglow, which was supposed to be due to a dissociative recombination process.

The total rate of emitted photons was significantly lower than the effective recombination rate, in particular for gas pressures above 400 Torr. At pressures lower than 400 Torr the afterglow spectrum was dominated by intense He_2 bands, which were related to the recombination of He_2^+ and He_3^+ ions. For pressures above 400 Torr a gradual change in the relative ion concentrations from He_2^+ being the dominant ion to He_4^+ is predicted from mass spectrometric results reported for lower pressures. Where this change should occur, the spectral lines from the lower excited atomic levels became more intense than the molecular band radiation during the early afterglow, and we propose that this line radiation originates from the recombination of He_4^+ ions.

Evidence for dissociative recombination terminating directly in the atomic metastable 2^3S state was found, while the concentration of molecular metastables was surprisingly low.

The influence of an electron temperature elevation on the afterglow light emission in the visible wavelength region could be described as a $T_e^{-\chi}$ dependence, where for the atomic lines originating from the quantum levels n = 3 χ is rather small, $0.0 < \chi < 0.35$, while for the molecular bands $0.78 < \chi < 1.10$. The intensity of the infrared 10 830 Å line increased with electron temperature due to electronic excitation of the 2^3P state from the metastable 2^3S state.

ACKNOWLEDGEMENT

The authors wish to express their gratitude to the initiator of these experiments, Dr. F. Robben, for many stimulating and helpful discussions during the course of this work.

REFERENCES

1. BATES, D.R., KINGSTON, A.E. and McWHIRTER, R.W.P., Recombination between electrons and atomic ions. 1 and 2. Proc. Roy. Soc. 267A (1962), p. 297 and 270A (1962), p. 155.

2. COLLINS, C.B. and ROBERTSON, W.W., Helium afterglow. 2. Molecular spectrum. J. Chem. Phys. 40 (1964), p. 2208.

3. STEVEFELT, J., Recombination measurements in helium plasmas at pressures 100 - 760 Torr. Phenomena in ionized gases. 9th Int. Conf. Bucharest. Sept. 1 - 6, 1960. Bucharest 1969, p. 1.

4. BERLANDE, J., CHERET, M., DELOCHE, R., GONFALONE, A., and MANUS, C., Pressure and electron density dependence of the electron-ion recombination coefficient in helium. Phys. Rev. A. 1 (1970), p. 887.

5. BATES, D.R. and KHARE, S.P., Recombination of positive ions and electrons in a dense neutral gas. Proc. Phys. Soc. 85 (1965), p. 231.

6. COLLINS, C.B., HICKS, H.S. and WELLS, W.E., Direct measurement of the dependence on electron density of the recombination rate coefficient of He_2^+ with electrons in a high-pressure helium plasma. Phys. Rev. A. 2 (1970), p. 797.

   Stabilization of the recombination of atomic and molecular ions in a high pressure helium afterglow. Phys. Rev. A. (To be published).

7. GUSINOW, M.A., GERBER, R.A and GERARDO, J.B., He_3^+ and He_4^+ in 300°K helium plasmas: their effect on recombination loss of electrons. Phys. Rev. Letters 25 (1970), p. 1248.

8. GERARDO, J.B. and GUSINOW, M.A., Electronic recombination of He_3^+. Phys. Rev. A 3 (1971), p. 255.

9. STEVEFELT, J., Spectroscopic study of recombination in the early afterglow of a helium plasma. 1968. (AE-311).

10. SPITZER Jr., L., Physics of fully ionized gases. 2 rev. ed. Interscience Publishers, New,York, 1962. Chap. 5.

11. KERR, D.E., LEFFEL, C.S. and HIRSH, M.N., Creation and destruction processes in low-energy helium plasmas. (Unpublished).

12. GERBER, R. A., SAUTER, G. F. and OSKAM, H. J.,
Studies of decaying helium plasmas.
Physica 32 (1966), p. 2173.

13. NILES, F. E. and ROBERTSON, W. W.,
Atomic emission of the helium afterglow.
J. Chem. Phys. 40 (1964), p. 3568.

14. COLLINS, C. B. and HURT, W. B.,
Late-time source of atomic light in the helium afterglow.
Phys. Rev. 177 (1969), p. 257.

15. COLLINS, C. B.,
Chemistry of the low pressure helium afterglow.
Phenomena in ionized gases. 9th Int. Conf. Bucharest.
Sept. 1 - 6, 1969, Bucharest 1969, p. 51.

16. PAKHOMOV, P. L. and FUGOL, I. Ya.,
Paired collisions of metastable atoms of helium in plasma.
Dokl. Akad. Nauk SSSR, 159 (1964), p. 57 (Soviet Phys. "Doklady", 9 (1965), p. 975).

17. BATES, D. R., BELL, K. L. and KINGSTON, A. E.,
Excited atoms in decaying optically thick plasmas.
Proc. Phys. Soc. 91 (1967), p. 288.

18. PHELPS, A. V.,
Absorption studies of helium metastable atoms and molecules.
Phys. Rev. 99 (1955), p. 1307.

19. GRYZINSKI, M.,
Classical theory of atomic collisions. I. Theory of inelastic collisions.
Phys. Rev. 138 (1965), p. A336.

CAPTIONS

Table 1. Relative intensities of lines belonging to the spectral series $n^3D - 2^3P$ for different gas pressures. In order to facilitate a comparison, the intensity of the $6^3D - 2^3P$ line has been normalized to unity.

Table 2. A comparison of the photon emission rates in atomic lines (I_{at}) and molecular bands (I_{mol}) with the effective recombination rate $\alpha_{eff} N_e^2$ for different gas pressures. Electron density is equal to 10^{18} m^{-3}. Also shown is the ratio α/α_{eff}, where α is defined by equation (6) in the text and the slopes of the straight lines in Figure 9. K = 1/280.

Figure 1. Simplified block diagram of the experimental apparatus.

Figure 2. A graph of the experimentally determined conductivity as a function of time in the afterglow. The gas pressure is 388 Torr, and the gas temperature near 300°K. The bars represent the estimated error of the measurement. The conductivity values are derived assuming a constant geometrical form factor which is measured only during the first 60 μsec of the afterglow.

Figure 3. The time variation of N_e^{-1} for five different gas pressures.

Figure 4. The sudden change in effective recombination rate coefficient, which occurs at 50 μsec delay time in the afterglow at a gas pressure of 383 Torr.

Figure 5. Effective recombination rate coefficients for different gas pressures. The straight line with slope equal to one represents

the results reported by Berlande et al. (Ref. (4)) for the low electron density limit. The dotted bar illustrates results given by Collins (Ref. (6)) for varying electron density, and the triangles represent results previously reported from this experiment (Ref. (3)). The solid bars illustrates the present measurements.

Figure 6. Variation of the 5876 Å line intensity with the electron density at different gas pressures.

Figure 7. Variation of the 4650 Å band intensity with the electron density at different gas pressures.

Figure 8. Relationship between the 5876 Å line and the 4650 Å band intensities at different gas pressures.

Figure 9. A graph of the function $(I_{4653})^{-1/2}$ of time for different gas pressures.

Figure 10. The pressure variation of the time derivative of the function $(I_{4653})^{-1/2}$. Solid bars represent the present experiment, dotted bar the result given in Ref. (6).

Figure 11. The decay of metastable 2^3S concentration with time for different gas pressures.

Figure 12. Variation with electron temperature of the light emission in some spectral features. Full circles represent the 10 830 Å line, open circles the 5876 Å line, squares represent the 4653 Å Q(7) rotational line, and triangles denote the impurity H_β line. All spectral line intensities are normalized to unity for zero field. The deviations from the straight lines in the figure may be due to an assumed electron temperature which

is too small for weak electric fields. The gas pressure is 88 Torr, and the gas temperature 520°K.

Figure 13. Time variation of the light emission in the 5876 Å and 10 830 Å atomic lines, and in the 4653 Å rotational line of the 4650 Å He_2 band, when a 10 μsec heating pulse is applied (solid lines). The dashed lines indicate light emission in the absence of external heating. The gas pressure is 165 Torr, and the gas temperature 510°K. During the heating pulse, the calculated electron temperature is 2300°K.

Figure 14. Calculated relative concentrations of the molecular helium ions He_2^+, He_3^+, and He_4^+ in equilibrium at 300°K gas temperature, for different gas pressures. Equilibrium constants are taken from Gusinow et al. (Ref. (7)).

Table 1

Spectral line	Gas pressure, (Torr)			
	6.7	200	307	464
$3^3D - 2^3P$	61.4	125	170	330
$4^3D - 2^3P$	11.1	12.0	9.2	8.3
$5^3D - 2^3P$	2.9	3.1	2.5	2.3
$6^3D - 2^3P$	1.0	1.0	1.0	1.0

Table 2

Pressure (Torr)	I_{at} ($m^{-3}sec^{-1}$)	I_{mol} ($m^{-3}sec^{-1}$)	$\alpha_{eff} N_e^2$ ($m^{-3}sec^{-1}$)	α/α_{eff}
200	$1.8 \cdot 10^{20}$	$3.6 \cdot 10^{21}$	$3.6 \cdot 10^{22}$	0.26
388	$6.9 \cdot 10^{21}$	$9.8 \cdot 10^{21}$	$5.5 \cdot 10^{22}$	0.19
464	$1.5 \cdot 10^{22}$	$7.3 \cdot 10^{21}$	$1.1 \cdot 10^{23}$	0.02
578	$1.9 \cdot 10^{21}$	$1.6 \cdot 10^{21}$	$9.0 \cdot 10^{22}$	-

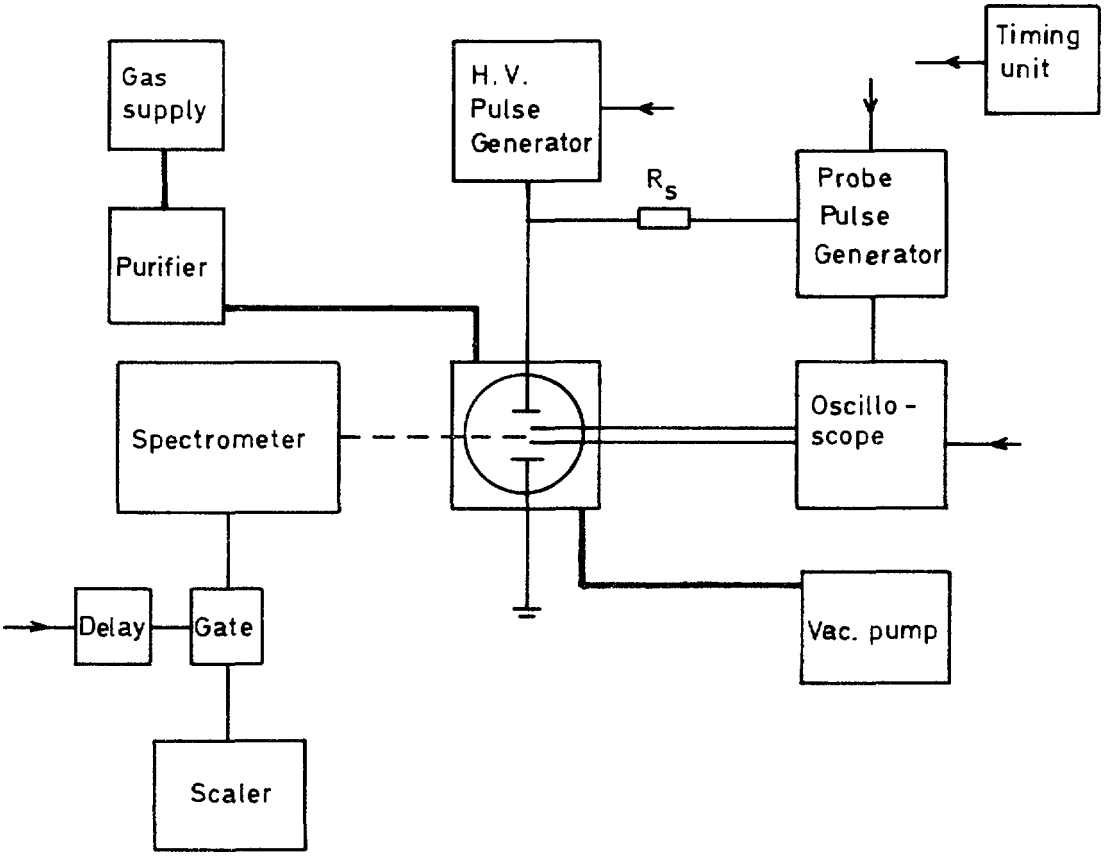
Gas supply
Purifier
H.V. Pulse Generator
R_s
Timing unit
Probe Pulse Generator
Spectrometer
Oscillo - scope
Delay
Gate
Scaler
Vac. pump

Fig. 1.

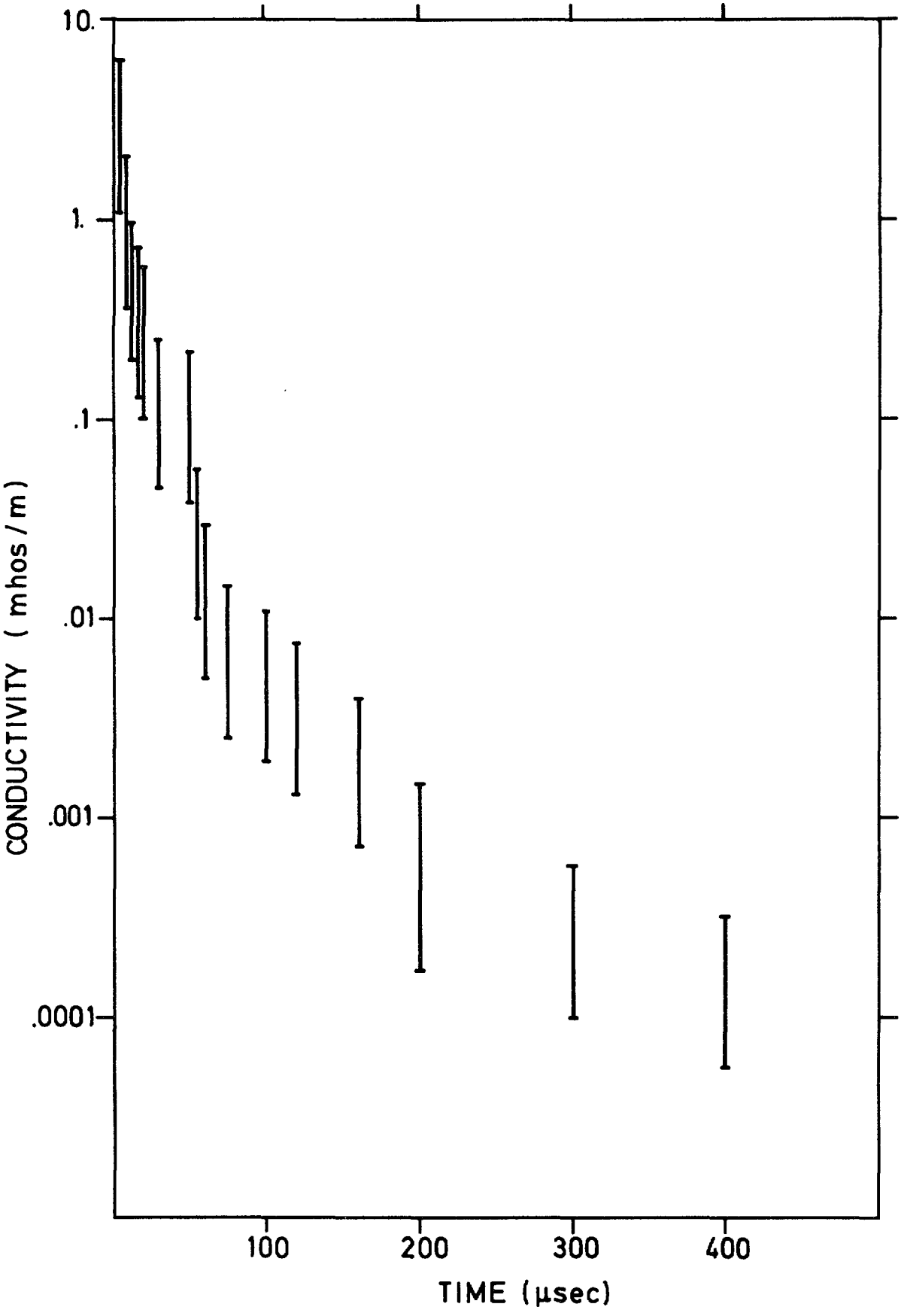
10.
1.
.1
.01
.001
.0001
CONDUCTIVITY (mhos / m)
100
200
300
400
TIME (μsec)

Fig. 2.

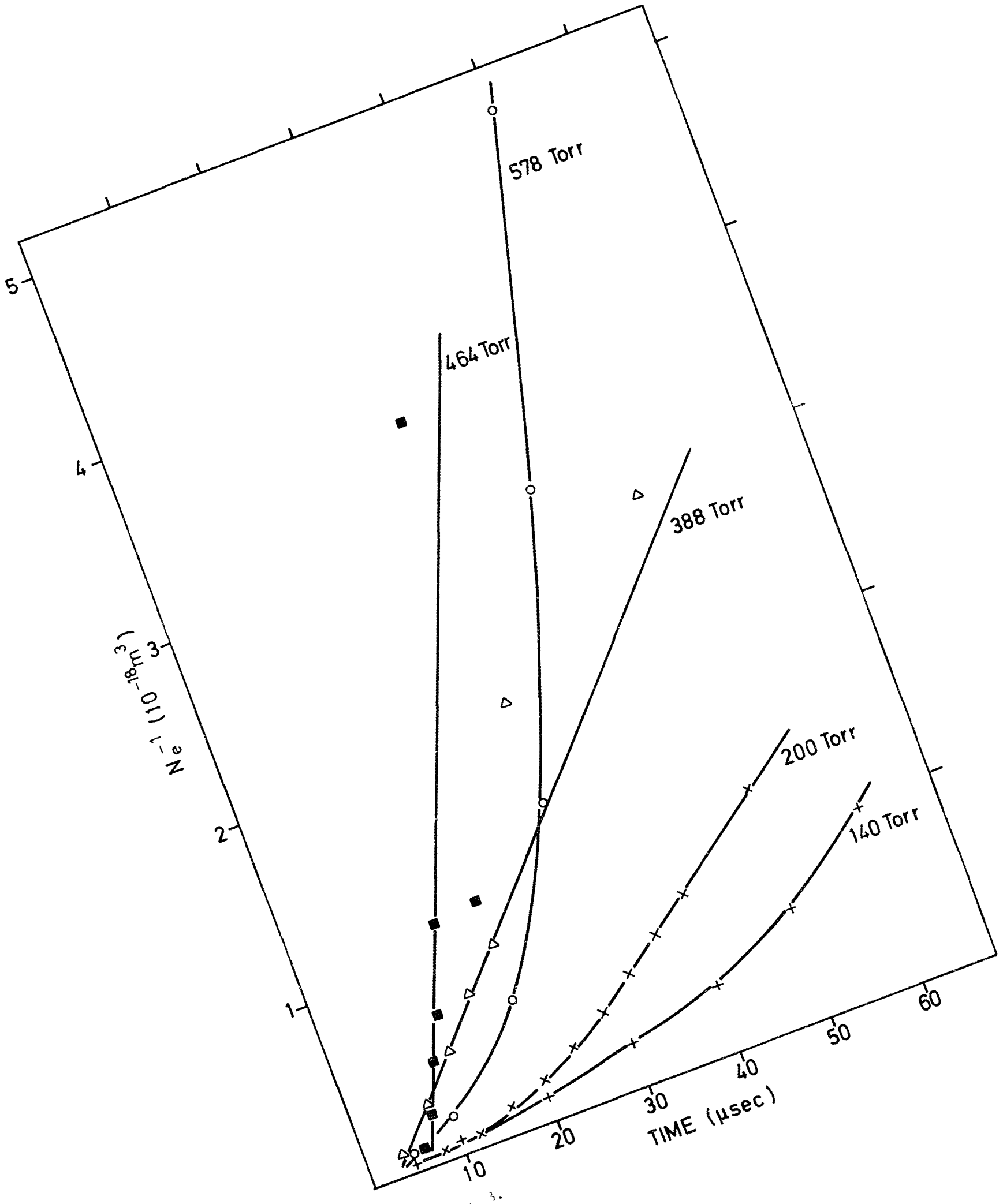
578 Torr
464 Torr
388 Torr
200 Torr
140 Torr
N_e^{-1} (10^{-18} cm^3)
TIME (μsec)
1
2
3
4
5
10
20
30
40
50
60

Fig. 3.

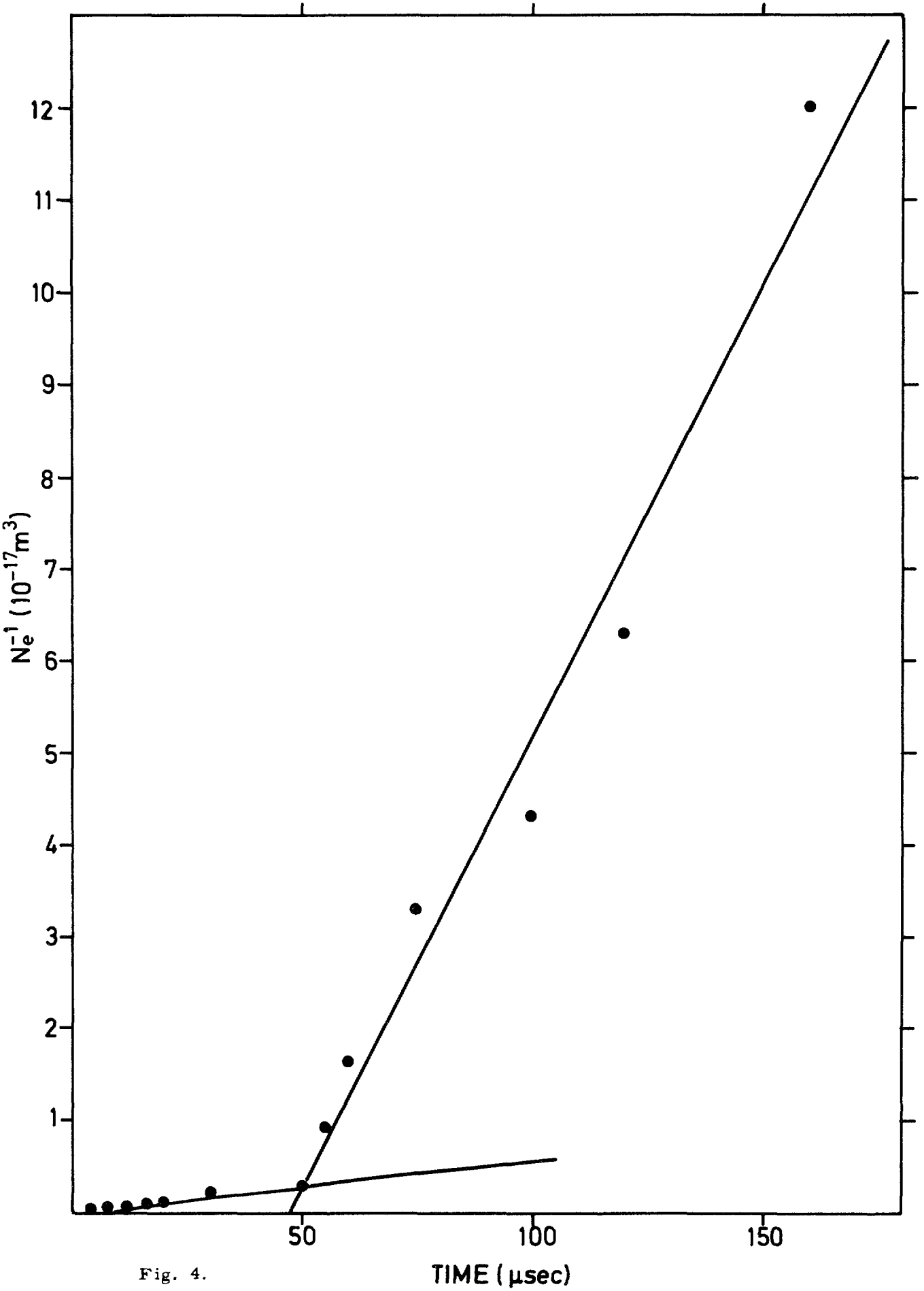

Fig. 4.

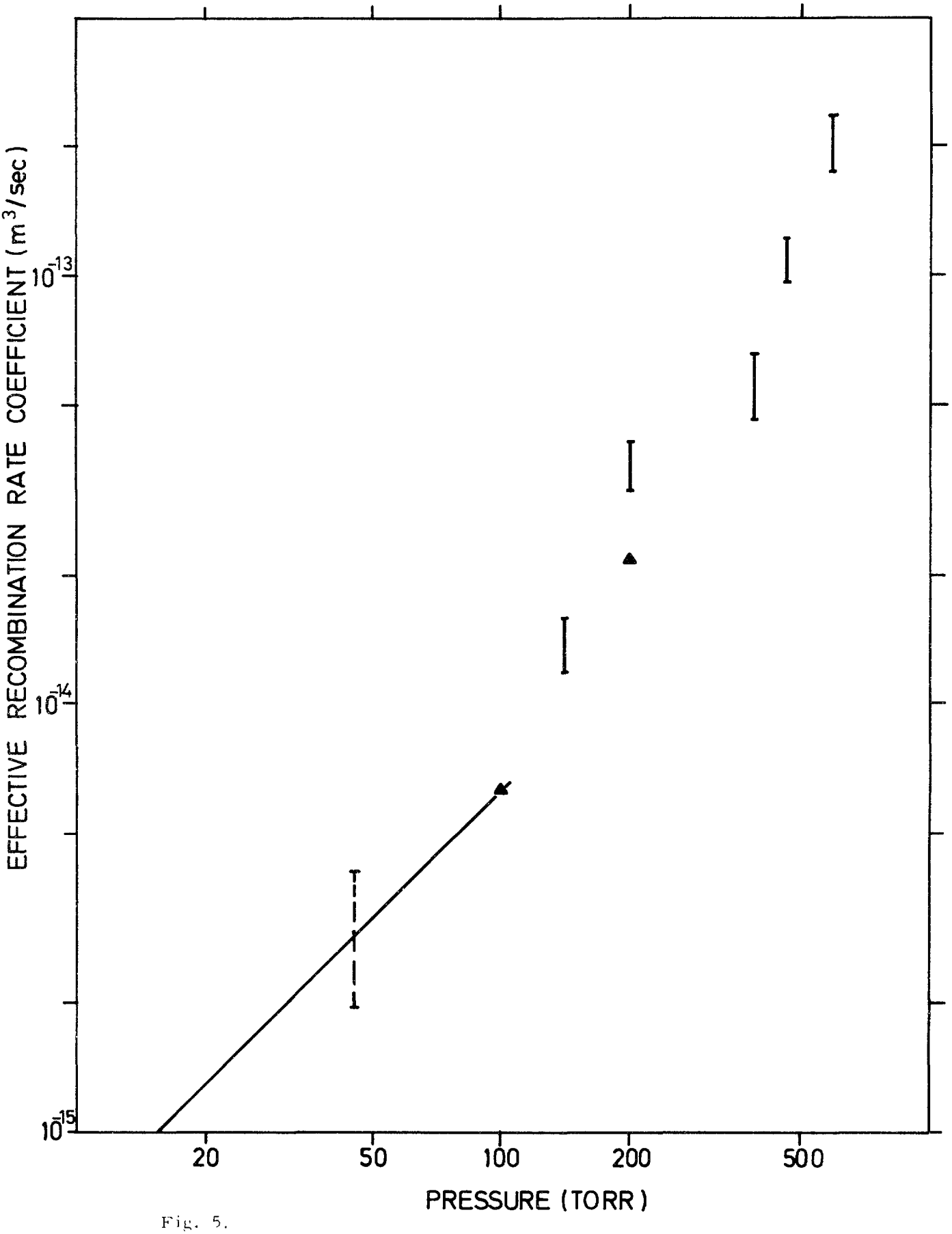
EFFECTIVE RECOMBINATION RATE COEFFICIENT (m^3/sec)
10^{-13}
10^{-14}
10^{-15}
20
50
100
200
500
PRESSURE (TORR)

Fig. 5.

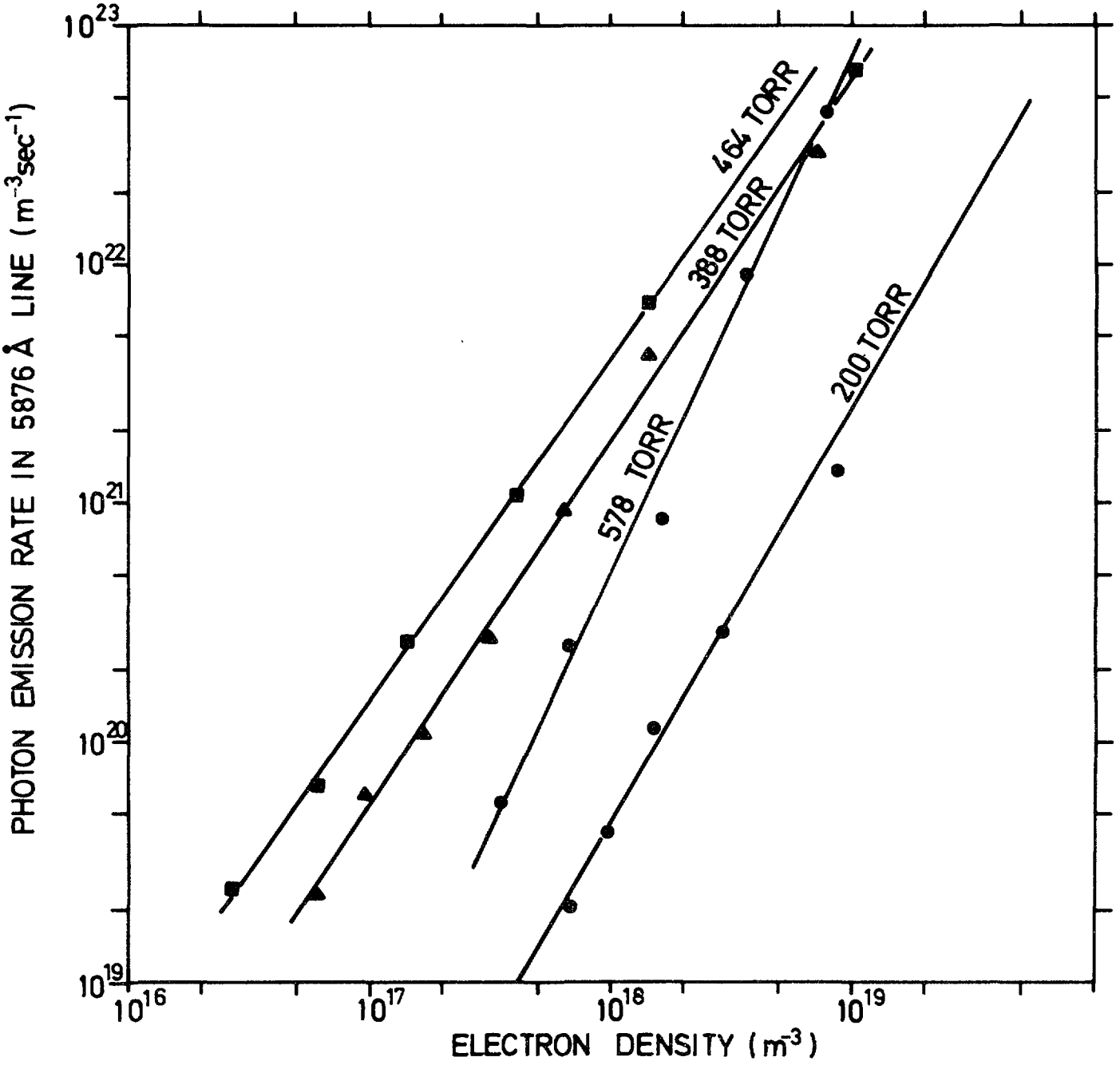
PHOTON EMISSION RATE IN 5876 Å LINE ($m^{-3}sec^{-1}$)
10^{23}
10^{22}
10^{21}
10^{20}
10^{19}
10^{16}
10^{17}
10^{18}
10^{19}
ELECTRON DENSITY (m^{-3})
464 TORR
388 TORR
578 TORR
200 TORR

Fig. 6.

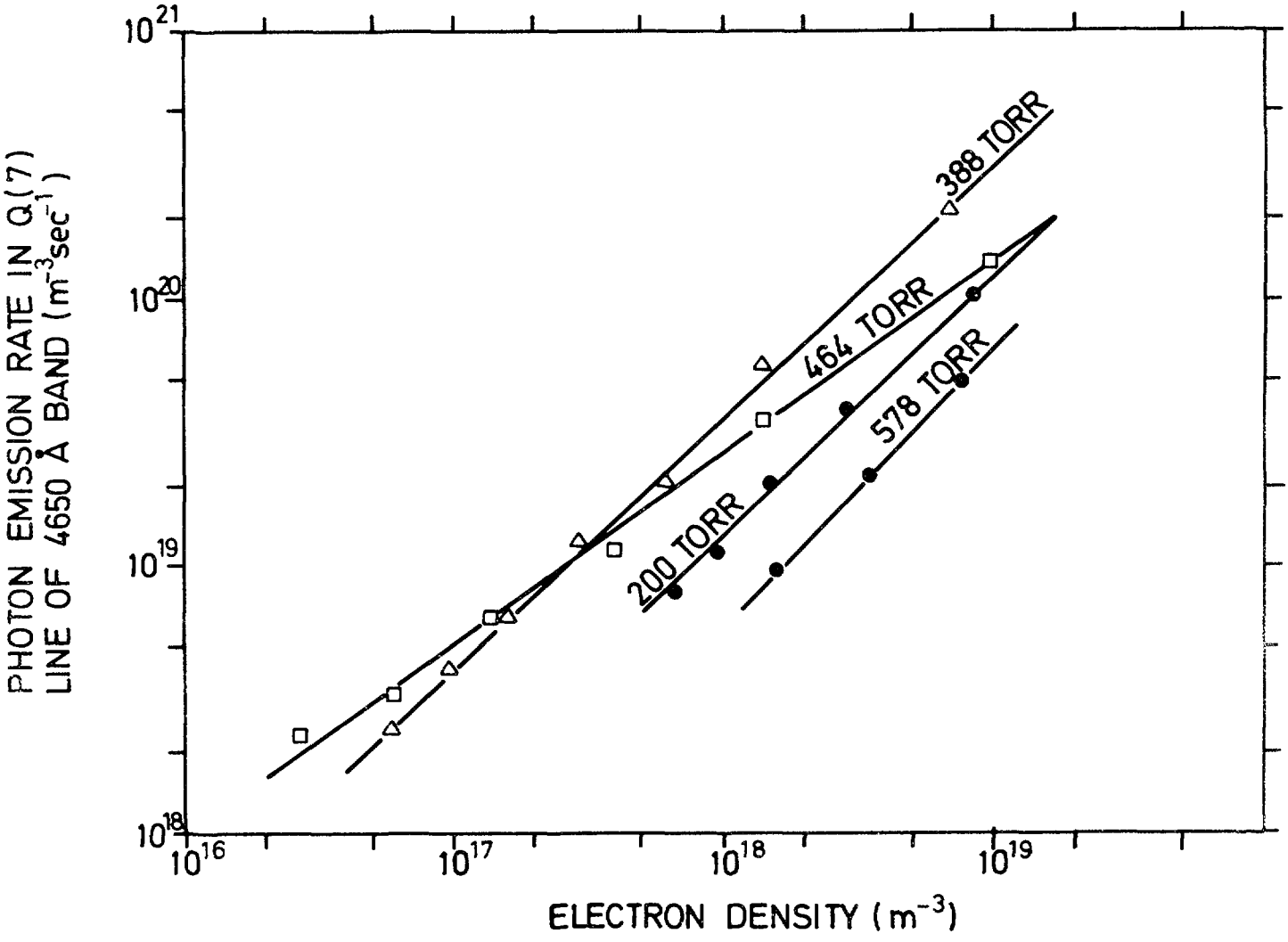
PHOTON EMISSION RATE IN Q(7)
LINE OF 4650 Å BAND ($m^{-3}sec^{-1}$)
10^{21}
10^{20}
10^{19}
10^{18}
388 TORR
464 TORR
578 TORR
200 TORR
10^{16}
10^{17}
10^{18}
10^{19}
ELECTRON DENSITY (m^{-3})

Fig. 7.

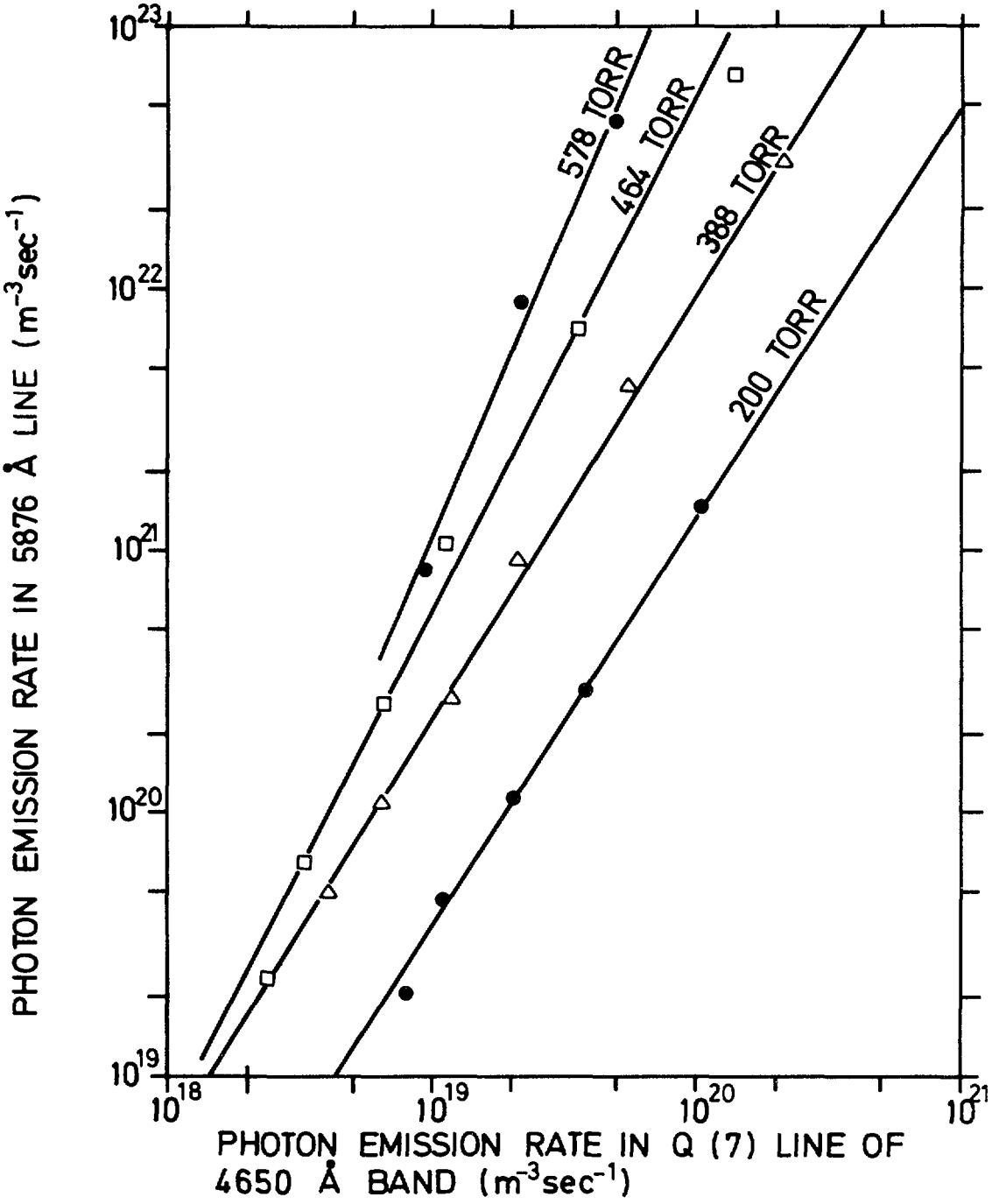
PHOTON EMISSION RATE IN 5876 Å LINE ($m^{-3}sec^{-1}$)
10^{23}
10^{22}
10^{21}
10^{20}
10^{19}
578 TORR
464 TORR
388 TORR
200 TORR
10^{18}
10^{19}
10^{20}
10^{21}
PHOTON EMISSION RATE IN Q (7) LINE OF 4650 Å BAND ($m^{-3}sec^{-1}$)

Fig. 8.

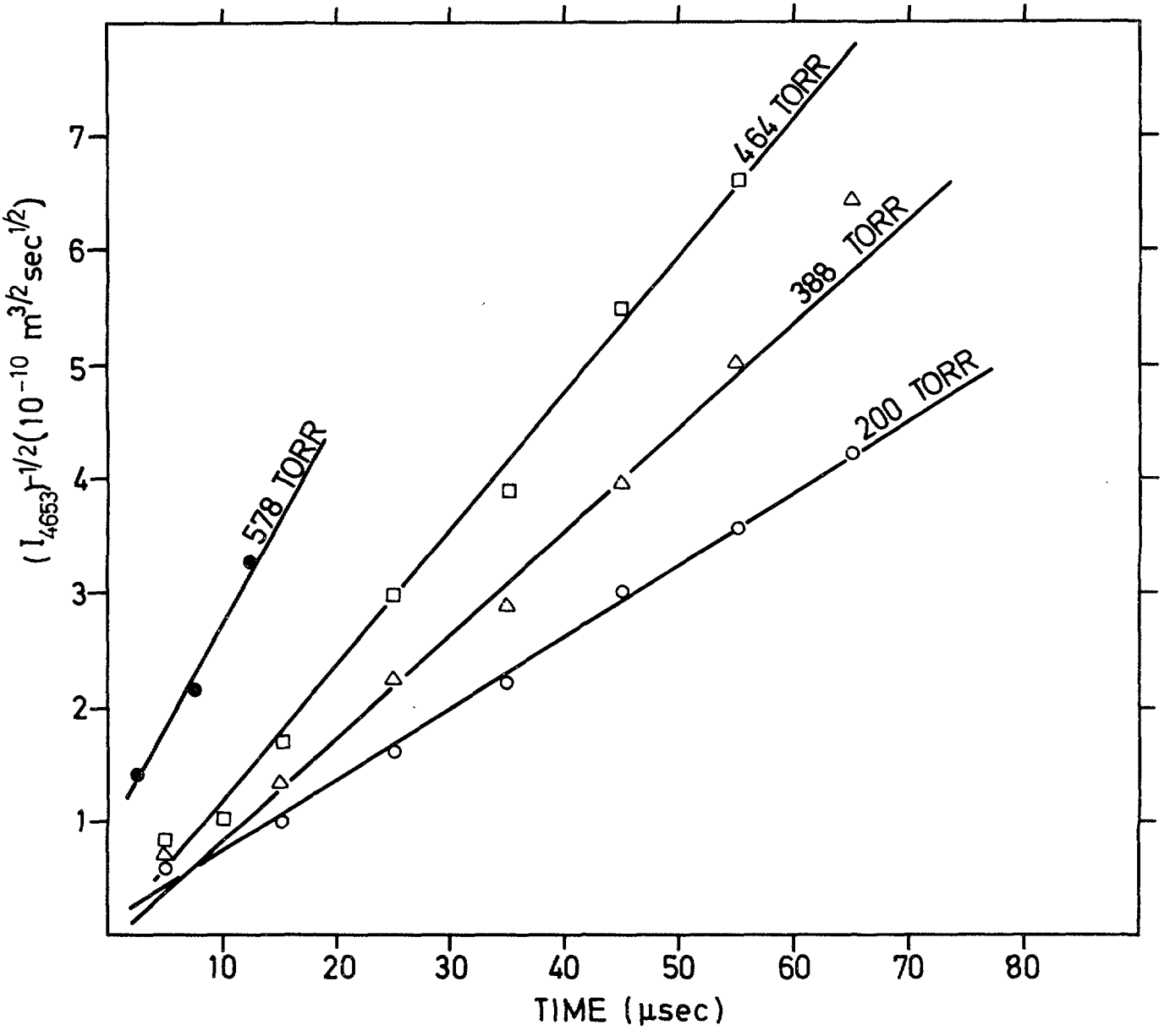
$(I_{4653})r^{1/2}(10^{-10}\ m^{3/2}sec^{1/2})$
TIME (μsec)
578 TORR
464 TORR
388 TORR
200 TORR
1
2
3
4
5
6
7
10
20
30
40
50
60
70
80

Fig. 9.

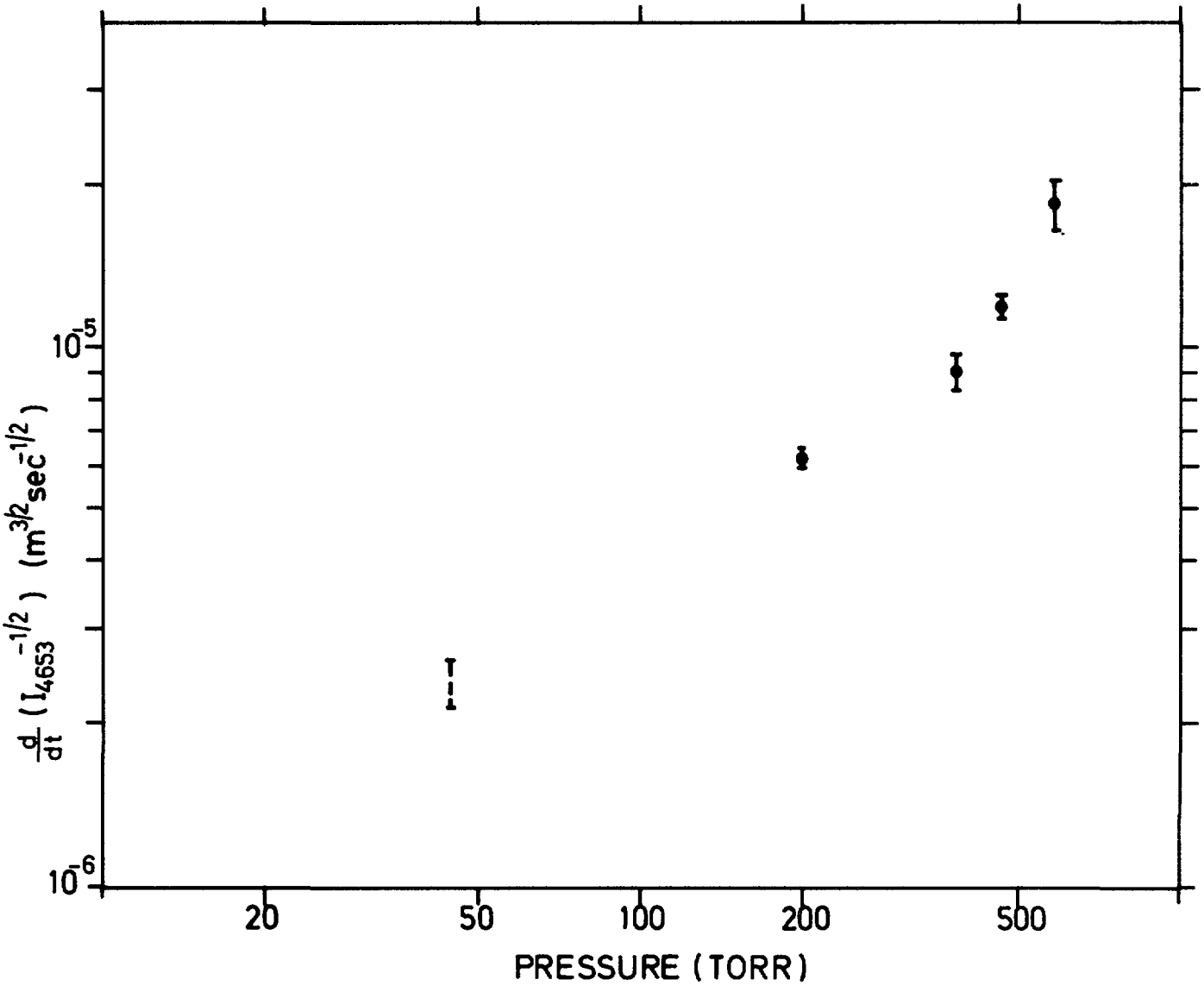
$\frac{d}{dt}(I_{4653}^{-1/2})$ $(m^{3/2}sec^{-1/2})$
10^{-5}
10^{-6}
20
50
100
200
500
PRESSURE (TORR)

Fig. 10.

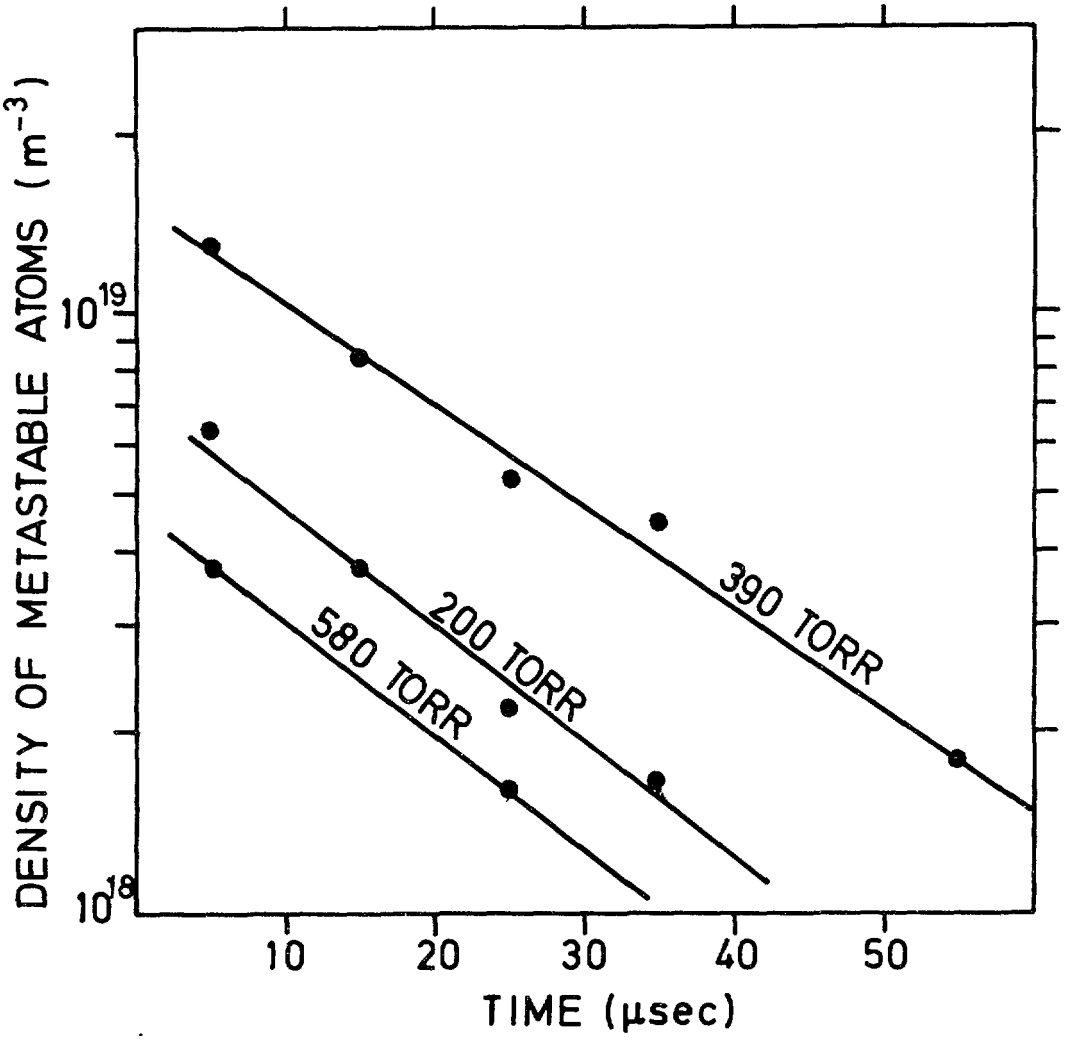
DENSITY OF METASTABLE ATOMS (m^{-3})
10^{19}
10^{18}
390 TORR
200 TORR
580 TORR
10
20
30
40
50
TIME (μsec)

Fig. 11.

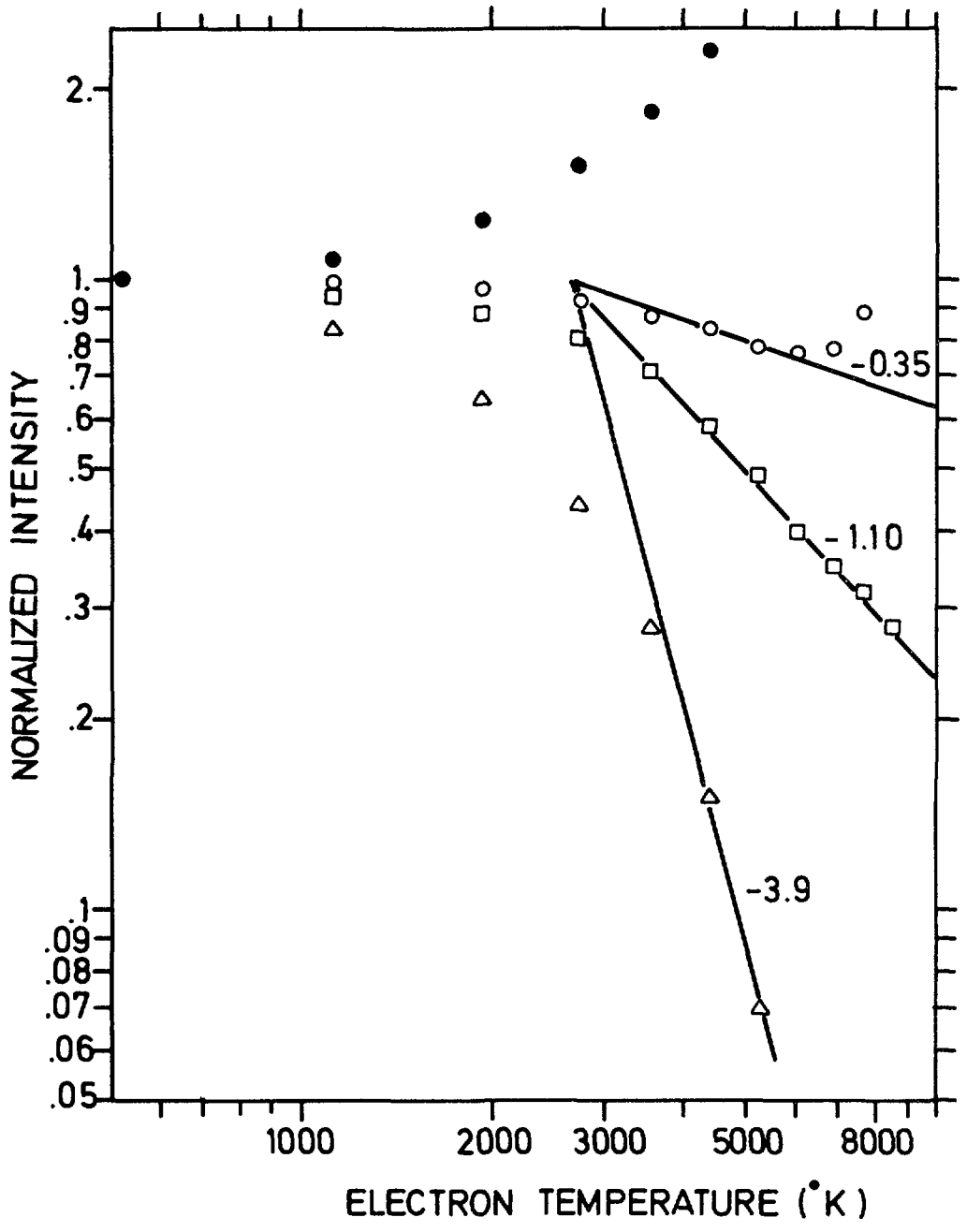
NORMALIZED INTENSITY
2.
1.
.9
.8
.7
.6
.5
.4
.3
.2
.1
.09
.08
.07
.06
.05
-0.35
-1.10
-3.9
1000
2000
3000
5000
8000
ELECTRON TEMPERATURE (°K)

Fig. 12.

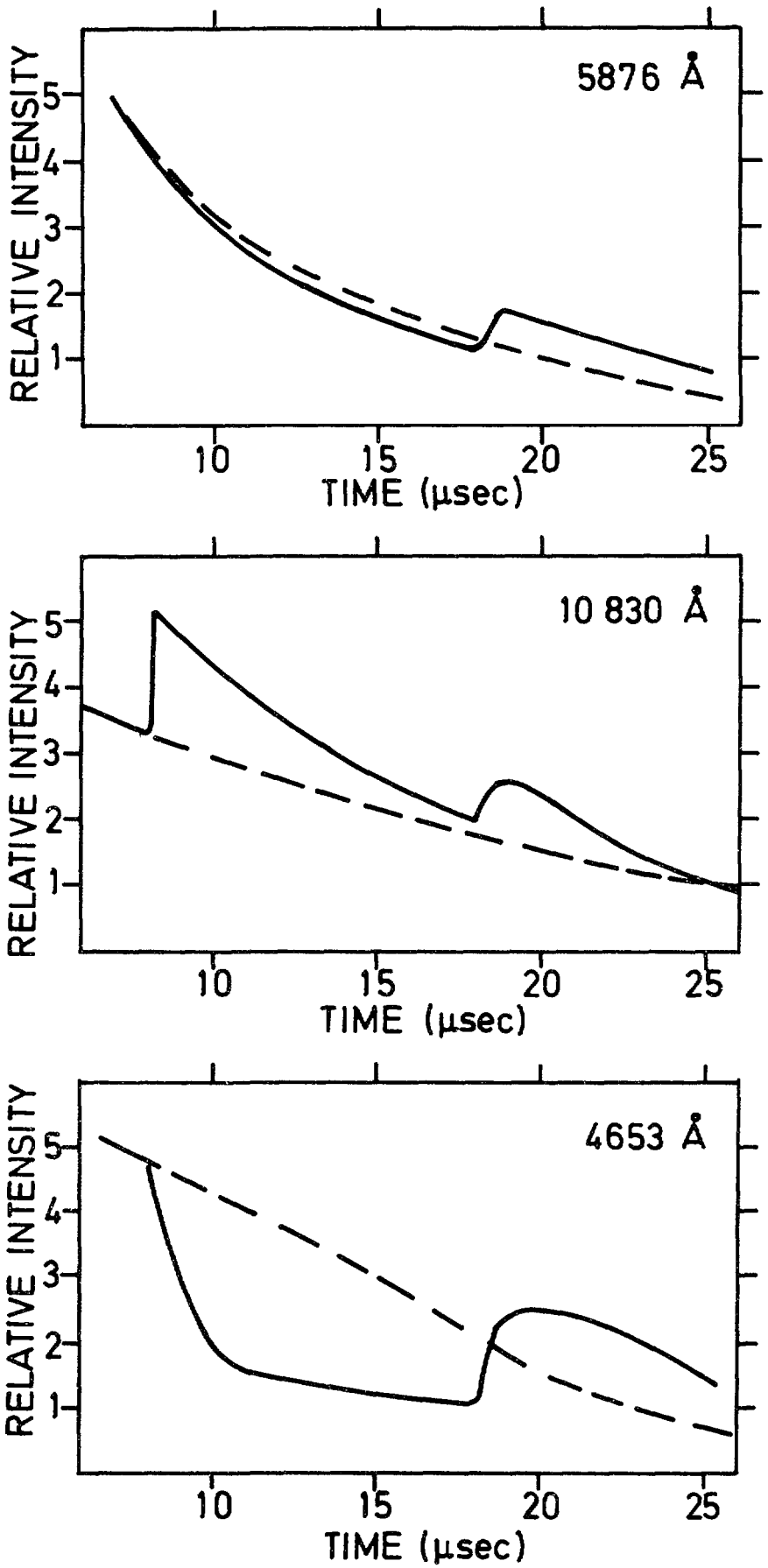
5876 Å
RELATIVE INTENSITY
1
2
3
4
5
10
15
20
25
TIME (μsec)
10 830 Å
RELATIVE INTENSITY
1
2
3
4
5
10
15
20
25
TIME (μsec)
4653 Å
RELATIVE INTENSITY
1
2
3
4
5
10
15
20
25
TIME (μsec)

Fig. 13.

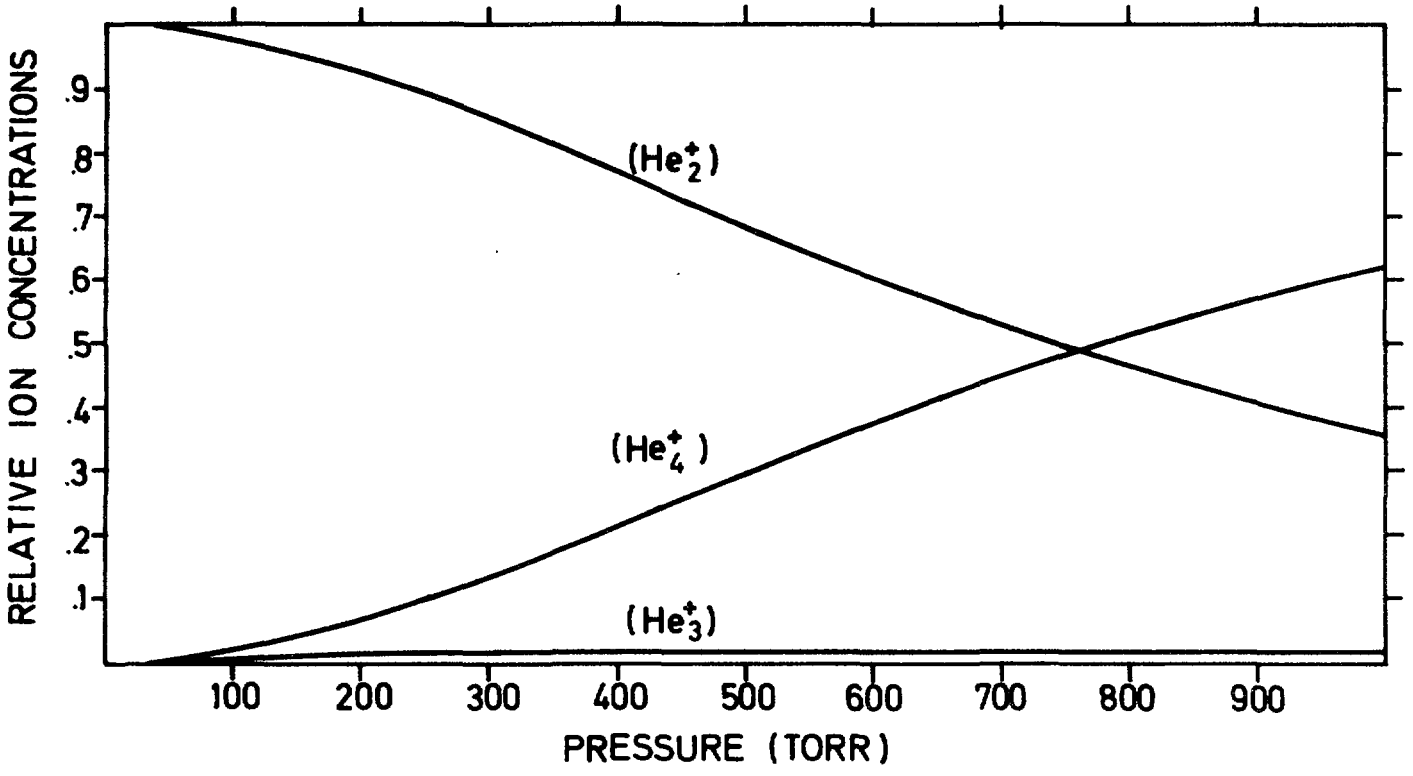
RELATIVE ION CONCENTRATIONS
.9
.8
.7
.6
.5
.4
.3
.2
.1
(He$_2^+$)
(He$_4^+$)
(He$_3^+$)
100
200
300
400
500
600
700
800
900
PRESSURE (TORR)

Fig. 14

LIST OF PUBLISHED AE-REPORTS

1–350 (See back cover earlier repports.)

351. A determination of the 2 200 m/s absorption cross section and resonance integral of arsenic by pile oscillator technique. By E. K. Sokolowski and R. Bladh. 1969. 14 p. Sw. cr. 10:–.

352. The decay of ^{191}Os. By S. G. Malmskog and A. Bäcklin. 1969. 24 p. Sw. cr. 10:–.

353. Diffusion from a ground level point source experiment with thermoluminescence dosimeters and Kr 85 as tracer substance. By Ch. Gyllander, S Hollman and U. Widemo. 1969. 23 p. Sw. cr. 10:–.

354. Progress report, FFN, October 1, – September 30, 1968. By T. Wiedling. 1969. 35 p. Sw. cr. 10:–.

355. Thermodynamic analysis of a supercritical mercury power cycle. By A S. Roberts, Jr. 1969. 25 p. Sw. cr. 10:–.

356. On the theory of compensation in lithium drifted semiconductor detectors By A. Lauber. 1969. 45 p. Sw. cr. 10:–.

357. Half-life measurements of levels in ^{75}As. By M. Höjeberg and S. G Malmskog. 1969. 14 p. Sw. cr. 10:–.

358. A non-linear digital computer model requiring short computation time for studies concerning the hydrodynamics of the BWR. By F. Reisch and G. Vayssier. 1969. 38 p. Sw. cr. 10:–.

359. Vanadium beta emission detectors for reactor in-core neutron monitoring. By I. Ö. Andersson and B. Söderlund. 1969. 26 p Sw. cr. 10:–

360. Progress report 1968. Nuclear chemistry. 1969. 38 p. Sw. cr. 10:–.

361. A half-life measurement of the 343.4 keV level in ^{175}Lu. By M. Höjeberg and S. G. Malmskog. 1969. 10 p. Sw. cr. 10:–.

362. The application of thermoluminescence dosimeters to studies of released activity distributions. By B-I. Rudén. 1969. 36 p. Sw. cr. 10:–.

363 Transition rates in ^{161}Dy. By V. Berg and S. G. Malmskog. 1969 32 p Sw. cr. 10:–.

364 Control rod reactivity measurements in the Ågesta reactor with the pulsed neutron method. By K. Björeus. 1969. 44 p. Sw. cr. 10:–.

365. On phonons in simple metals II. Calculated dispersion curves in aluminium. By R. Johnson and A. Westin. 1969. 124 p. Sw. cr. 10:–.

366. Neutron elastic scattering cross sections. Experimental data and optical model cross section calculations. A compilation of neutron data from the Studsvik neutron physics laboratory. By B. Holmqvist and T. Wiedling. 1969. 212 p. Sw. cr. 10:–.

367. Gamma radiation from fission fragments. Experimental apparatus – mass spectrum resolution. By J. Higbie. 1969. 50 p. Sw. cr. 10:–.

368. Scandinavian radiation chemistry meeting, Studsvik and Stockholm, September 17–19, 1969. By H. Christensen. 1969. 34.p. Sw. cr. 10:–.

369. Report on the personnel dosimetry at AB Atomenergi during 1968. By J. Carlsson and T. Wahlberg. 1969 10 p. Sw. cr. 10:–.

370. Absolute transition rates in ^{189}Ir. By S. G. Malmskog and V. Berg. 1969. 16 p. Sw. cr. 10:–.

371. Transition probabilities in the 1/2+(631) Band in ^{235}U. By M. Höjeberg and S. G. Malmskog. 1969. 18 p. Sw. cr. 10:–.

372. E2 and M1 transition probabilities in odd mass Hg nuclei. By V. Berg, A Bäcklin, B. Fogelberg and S. G. Malmskog. 1969. 19 p. Sw. cr. 10:–.

373. An experimental study of the accuracy of compensation in lithium drifted germanium detectors. By A. Lauber and B. Malmsten. 1969. 25 p. Sw. cr. 10:–.

374. Gamma radiation from fission fragments. By J. Higbie. 1969. 22 p. Sw. cr. 10:–.

375. Fast neutron elastic and inelastic scattering of vanadium. By B. Holmqvist, S. G. Johansson, G. Lodin and T. Wiedling. 1969. 48 p. Sw. cr. 10:–.

376. Experimental and theoretical dynamic study of the Ågesta nucler power station. By P. Å. Bliselius, H. Vollmer and F. Åkerhielm. 1969. 39 p Sw. cr. 10:–.

377. Studies of Redox equilibria at elevated temperatures 1. The estimation of equilibrium constants and standard potentials for aqueous systems up to 374°C. By D. Lewis. 1969. 47 p. Sw. cr. 10:–.

378. The whole body monitor HUGO II at Studsvik. Design and operation. By L Devell, I. Nilsson and L. Venner. 1970. 26 p. Sw. cr. 10:–.

279. ATOMSPHERIC DIFFUSION. Investigations at Studsvik and Agesta 1960–1963. By L-E. Hæggblom, Ch. Gyllander and U. Widemo. 1969. 91 p. Sw cr. 10:–.

380. An expansion method to unfold proton recoil spectra. By J. Kockum. 1970. 20 p. Sw. cr. 10:–.

381. The 93.54 keV lever ^{91}Sr, and evidence for 3-neutron states above N=50. By S. G. Malmskog and J. McDonald 1970. 24 p. Sw. cr. 10:–.

382. The low energy level structure of ^{191}Ir. By S. G. Malmskog, V. Berg, A. Bäcklin and G Hedin. 1970. 24 p Sw cr. 10:–.

383. The drinking rate of fish in the Skagerack and the Baltic. By J. E. Larsson. 1970. 16 p. Sw. cr. 10:–.

384. Lattice dynamics of Nacl, KCl, RbCl and RbF. By G. Raunio and S. Rolandson. 1970. 26 p. Sw. cr. 10:–.

385. A neutron elastic scattering study of chromium, iron and nickel in the energy region 1.77 to 2.76 MeV. By B. Holmqvist, S. G. Johansson, G. Lodin, M Salama and T. Wiedling. 1970. 26 p. Sw. cr. 10:–.

386. The decay of bound isobaric analogue states in ^{29}Si and ^{29}Si using (d. nγ) reactions. By L. Nilsson, A Nilsson and I. Bergqvist. 1970. 34 p. Sw. cr. 10–.

387. Transition probabilities in ^{189}Os. By S. G. Malmskog, V. Berg and A. Bäcklin. 1970 40 p. Sw. cr. 10:–.

388. Cross sections for high-energy gamma transition from MeV neutron capture in ^{206}Pb. By I. Bergqvist, B. Lundbarg and L. Nilsson. 1970. 16 p. Sw. cr. 10:–.

389. High-speed, automatic radiochemical separations for activation analysis in the biological and medical research laboratory. By K. Samsahl. 1970. 18 p. Sw. cr. 10:–.

390. Use of fission product Ru-106 gamma activity as a method for estimating the relative number of fission events in U-235 and Pu-239 in low-enriched fuel elements. By R. S. Forsyth and W. H. Blackadder. 1970. 26 p. Sw. cr. 10:–.

391. Half-life measurements in ^{134}I. By V. Berg and A. Höglund. 1970. 16 p Sw. cr. 10:–.

392. Measurement of the neutron spectra in FRO cores 5, 9 and PuB-5 using resonance sandwich detectors. By T. L. Andersson and M. N. Qazi. 1970. 30 p. Sw. cr. 10:–.

393. A gamma scanner using a Ge(Li) semi-conductor detector with the possibility of operation in anti-coincidence mode. By R. S. Forsyth and W. H. Blackadder. 1970. 22 p. Sw. cr. 10:–.

394. A study of the 190 keV transition in ^{141}La. By B. Berg, A. Höglund and B. Fogelberg. 1970 22 p. Sw cr. 10:–.

395. Magnetoacoustic waves and instabilities in a Hall-effect-dominiated plasma. By S. Palmgren 1970. 20 p Sw. cr. 10:–.

396. A new boron analysis method. By J. Weitman, N. Dåverhög and S. Farvolden. 1970 26 p. Sw. cr. 10:–.

397. Progress report 1969. Nuclear chemistry. 1970. 39 p. Sw. cr. 10:–.

398. Prompt gamma radiation from fragments in the thermal fission of ^{235}U. By H. Albinsson and L. Lindow. 1970. 48 p. Sw. cr. 10:–.

399. Analysis of pulsed source experiments performed in copper-reflected fast assemblies. By J. Kockum. 1970. 32 p. Sw. cr. 10:–.

400. Table of half-lives for excited nuclear levels. By S G. Malmskog. 1970 33 p. Sw. cr. 10:–.

401. Needle type solid state detectors for in vivo measurement of tracer activity. By A. Lauber, M. Wolgast. 1970. 43 p. Sw. cr. 10:–.

402. Application of pseudo-random signals to the Ågesta nuclear power station By P-Å. Bliselius. 1970. 30 p. Sw. cr. 10:–.

403 Studies of redox equilibria at elevated temperatures 2. An automatic divided-function autoclave and cell with flowing liquid junction for electrochemical measurements on aqueous systems. By. K. Johnsson, D. Lewis and M. de Pourbaix. 1970. 38 p. Sw. cr. 10:–.

404. Reduction of noise in closed loop servo systems. By K. Nygaard. 1970. 23 p Sw. cr. 10:–

405. Spectral parameters in water-moderated lattices. A survey of experimental data with the aid of two-group formulae. By E. K. Sokolowski. 1970. 22 p. Sw. cr. 10:–.

406. The decay of optically thick helium plasmas, taking into account ionizing collisions between metastable atoms or molecules. By J. Stevefelt. 1970. 18 p. Sw. cr. 10:–.

407. Zooplankton from Lake Magelungen, Central Sweden 1960-63. By E. Almquist. 1970. 62 p. Sw. cr. 10:–.

408. A method for calculating the washout of elemental iodine by water sprays. By E. Bachofner and R. Hesböl. 1970. 24 p. Sw. cr. 10:–.

409. X-ray powder diffraction with Guinier–Hägg focusing cameras. By A. Brown. 1970. 102 p. Sw. cr. 10:–.

410. General physic section Progress report. Fiscal year 1969/70. By J. Braun. 1970. 92 p. Sw. cr. 10:–.

411. In-pile determination of the thermal conductivity of UO_2 in the range 500–2 500 degrees centigrade. By J-Å Gyllander. 1971. 70 p. Sw. cr. 10:–.

412. A study of the ring test for determination of transverse ductility of fuel element canning. By G. Anevi and G. Östberg. 1971. 17 p. Sw. cr. 15:–.

413. Pulse radiolysis of Aqueous Solutions of aniline and substituted anilines. By H. C. Christensen. 1971. 40 p. Sw. cr. 15:–.

414. Radiolysis of aqueous toluene solutions. By H. C. Christensen and R. Gustafson. 1971. 20 p. Sw. cr. 15:–.

415. The influence of powder characteristics on process and product parameters in UO_2 pelletization. By U. Runfors. 1971. 32 p. Sw. cr. 15:–.

416. Quantitative assay of Pu239 and Pu240 by neutron transmission measurements. By E. Johansson. 1971. 26 p. Sw. cr 15:–.

417. Yield of prompt gamma radiation in slow-neutron induced fission of ^{235}U as a function of the total fragment kinetic energy. By H. Albinsson. 1971. 38 p. Sw. cr. 15:–.

418. Measurements of the spectral light emission from decaying high pressure helium plasmas. By J. Stevefelt and J. Johansson. 1971. 48 p. Sw. cr. 15:–.

List of published AES-reports (In Swedish)

1 Analysis by means of gamma spectrometry. By D. Brune. 1961. 10 p. Sw. cr. 6:–.

2. Irradiation changes and neutron atmosphere in reactor pressure vessels-some points of view. By M. Grounes 1962. 33 p. Sw. cr. 6:–.

3. Study of the elongation limit in mild steel. By G. Östberg and R. Attermo. 1963. 17 p Sw cr. 6:–.

4. Technical purchasing in the reactor field. By Erik Jonson. 1963. 64 p. Sw. cr 8:–.

5 Ågesta nuclear power station. Summary of technical data, descriptions, etc for the reactor. By B. Lilliehöök. 1964. 336 p. Sw. cr. 15:–.

6 Atom Day 1965. Summary of lectures and discussions. By S. Sandström. 1966 321 p. Sw. cr. 15:–.

7 Building materials containing radium considered from the radiation protection point of view. By Stig O. W. Bergström and Tor Wahlberg. 1967. 26 p. Sw. cr. 10:–

Additional copies available from the Library of AB Atomenergi, Fack, S-611 01 Nyköping 1, Sweden.

EOS-tryckerierna, Stockholm 1971